Design and Synthesis of Fluoroquinophenoxazines That Interact with Human Telomeric G-Quadruplexes and Their Biological Effects[1]

Wenhu Duan, Anupama Rangan, Hariprasad Vankayalapati, et al.

Mol Cancer Ther 2001;1:103-120.

Design and Synthesis of Fluoroquinophenoxazines That Interact with Human Telomeric G-Quadruplexes and Their Biological Effects[1]

Wenhu Duan,[2,3] Anupama Rangan,[2] Hariprasad Vankayalapati,[2,3] Mu-Yong Kim,[3] Qingping Zeng,[4] Daekyu Sun, Haiyong Han, Oleg Yu. Fedoroff,[5] David Nishioka, Sun Young Rha,[6] Elzbieta Izbicka, Daniel D. Von Hoff, and Laurence H. Hurley[3,7,8]

College of Pharmacy, The University of Texas, Austin, Texas 78712 [W. D., A. R., M-Y. K., Q. Z., O. Y. F., L. H. H.]; Institute for Drug Development, San Antonio, Texas 78245 [D. S., S. Y. R., E. I., D. D. V. H.]; Department of Biology, Georgetown University, Washington, DC 20057 [D. N.]; and Arizona Cancer Center, Tucson, Arizona 85724 [H. H., D. D. V. H., L. H. H.]

Abstract

In this study we have identified a new structural motif for a ligand with G-quadruplex interaction that results in biological effects associated with G-quadruplex-interactive compounds. Fluoroquinolones have been reported to possess weak telomerase inhibitory activity in addition to their better known bacterial gyrase poisoning. Starting with a fluoroquinobenzoxazine, which has modest potency in a human topoisomerase II assay, we have designed a more potent inhibitor of telomerase that has lost its topoisomerase II poisoning activity. This fluoroquinophenoxazine (FQP) interacts with G-quadruplex structures to inhibit the progression of Taq polymerase in a G-quadruplex polymerase stop assay. In addition, we demonstrate by ^{1}H NMR studies that this compound interacts with telomeric G-quadruplex structures by external stacking to the G-tetrad with both the unimolecular fold-over and the parallel G-quadruplex structures. A photocleavage assay confirms the FQP interaction site, which is located off center of the external tetrad but within the loop region. Molecular modeling using simulated annealing was performed on the FQP-parallel G-quadruplex complex to determine the optimum FQP orientation and key molecular interactions with the telomeric G-quadruplex structure. On the basis of the results of these studies, two additional FQP analogues were synthesized, which were designed to test the importance of these key interactions. These analogues were evaluated in the Taq polymerase stop assay for G-quadruplex interaction. The data from this study and the biological evaluation of these three FQPs, using cytotoxicity and a sea urchin embryo system, were in accord with the predicted more potent telomeric G-quadruplex interactions of the initial lead compound and one of the analogues. On the basis of these structural and biological studies, the design of more potent and selective telomeric G-quadruplex-interactive compounds can be envisaged.

Introduction

Fluoroquinolones are best known therapeutically as bacterial gyrase inhibitors (1, 2) but more recently have also been demonstrated to be active against eukaryotic topoisomerase II, either as catalytic inhibitors or topoisomerase II poisons (3), or as telomerase inhibitors (4). One such group of compounds, the quinobenzoxazines, typified by A-62176 (Fig. 1*B*), has served as a starting point for the design of more potent topoisomerase II inhibitors using a structure-based approach (5). The extended aromatic conjugation system of A-62176 suggested to us that quinobenzoxazines may also intercalate with the more expansive system of G-quadruplex DNA and thereby be telomerase inhibitors in parallel with other G-quadruplex-interactive compounds, such as the anthraquinones (6–10), cationic porphyrins (11–13),[9] piperazines (14), ethidium compounds, (15), and a pentacyclicacridinium compound (16). After we started this project, an independent report that bacterial quinolones may be weak telomerase inhibitors (4) also supported the idea that a ring-extended fluoroquinolone would be a more potent telomerase inhibitor.

G-quadruplexes (Fig. 1*A)* were first identified in 1962 (17); however, their possible biological significance was only suggested starting in the late 1980s (18–23), and they were first proposed to be potential targets for drug design in 1989 (24). The existence of chaperone proteins that facilitate their formation (25–27), G-quadruplex binding proteins that recog-

Received 8/17/01; revised 9/21/01; accepted 10/2/01.
The costs of publication of this article were defrayed in part by the payment of page charges. This article must therefore be hereby marked *advertisement* in accordance with 18 U.S.C. Section 1734 solely to indicate this fact.
[1] Supported by NIH Grants CA88310 and CA67760.
[2] These authors contributed equally to this paper.
[3] Present address: College of Pharmacy, The University of Arizona, Tucson, AZ 85721.
[4] Present address: Monsanto Co., St. Louis, MO 63167.
[5] Present address: Department of Biomolecular Sciences, University of Manchester Institute of Science and Technology, Manchester M60 1QD, England.
[6] Present address: Cancer Metastasis Research Center, Yonsei University College of Medicine, Seoul, Korea.
[7] Present address: College of Pharmacy and Department of Chemistry, The University of Arizona, Tucson, AZ 85721 and Arizona Cancer Center, 1515 North Campbell Avenue, Tucson, AZ 85724.
[8] To whom requests for reprints should be addressed, at Arizona Cancer Center, 1515 N. Campbell Ave., Tucson, AZ 85724. Phone: 520-626-5622; Fax: 520-626-5623; E-mail: hurley@pharmacy.arizona.edu.

[9] D-F. Shi, R. T. Wheelhouse, D. Sun, and L. H. Hurley. Quadruplex-interactive agents as telomerase inhibitors: synthesis of porphyrins and structure-activity relationship for the inhibition of telomerase. J. Med. Chem., in press, 2001.

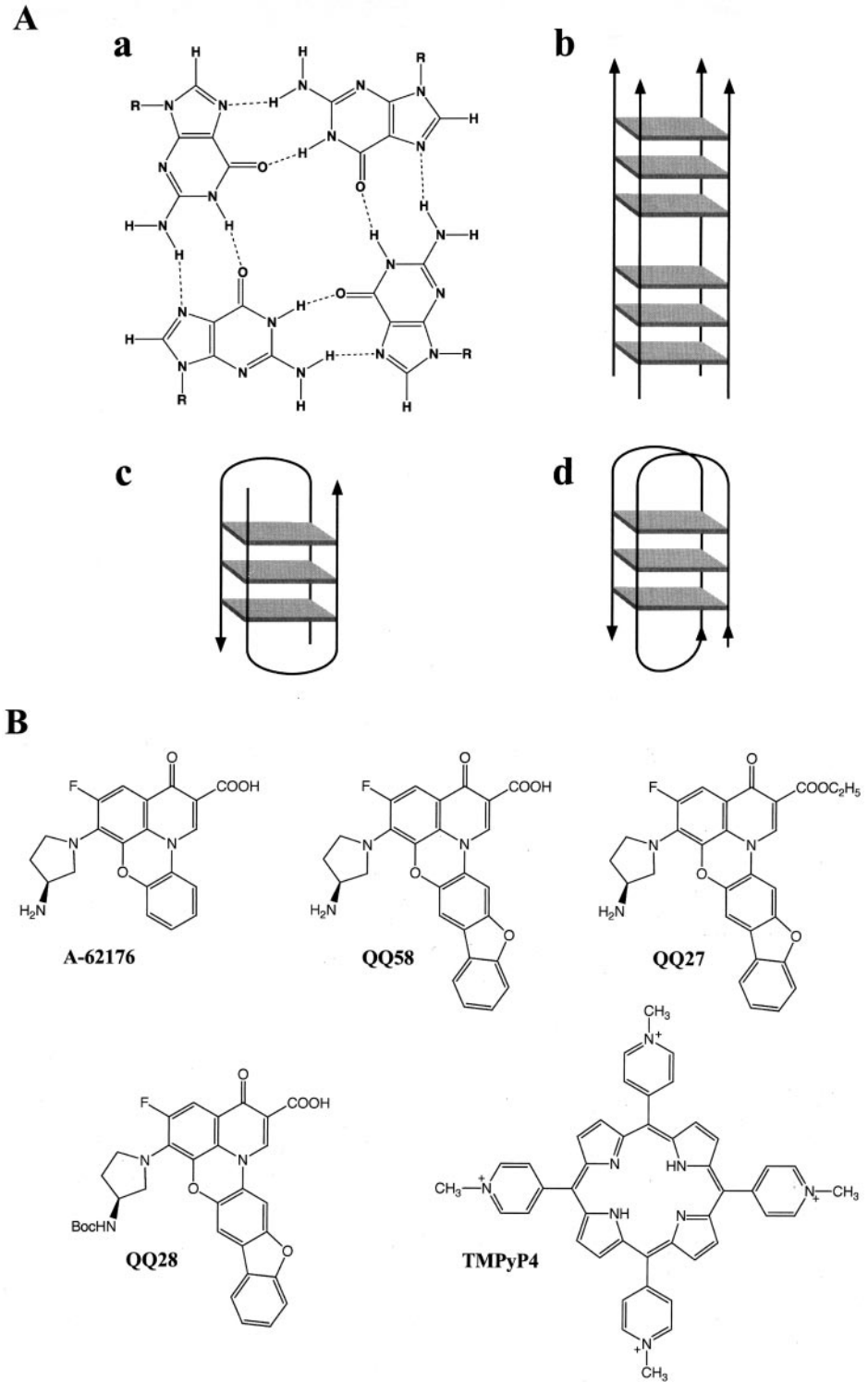

Fig. 1. *A,* G-tetrad and G-quadruplexes. *Panel a,* four guanine residues forming a planar structure G-tetrad through Hoogsteen hydrogen bonding. *Panel b,* a parallel G-quadruplex model. *Panel c,* an intermolecular antiparallel G-quadruplex model. *Panel d,* an intramolecular basket G-quadruplex model. Each parallelogram in *panels b–d* represents a G-tetrad. *B,* structures of the topoisomerase II-interactive compound (A-62176) and G-quadruplex-interactive compounds QQ58, QQ27, QQ28, and TMPyP4.

nize these structures (25, 28–31), and G-quadruplex-selective helicases (32–34) that unwind these structures make their existence *in vivo* in human cells a real possibility. Recently their *in vivo* existence in ciliates has been supported by antibody studies (35).

G-quadruplex-interactive compounds have aroused more interest recently because it has been demonstrated that these compounds not only inhibit telomerase in cell-free (6, 9) and in *in vitro* systems (36) but also cause telomere shortening and cell crisis in cancer cells

(14).[10] A number of reviews on G-quadruplex and their targeting by small molecules have appeared recently (37–45).

In this contribution we demonstrate that QQ58 (Fig. 1*B*), a FQP[11] that lacks bacterial gyrase or topoisomerase II poisoning activity, is able to bind to G-quadruplex structures and, by doing so, inhibit telomerase. Structural insight into the interactions of this compound with both intermolecular and intramolecular G-quadruplex structures has been obtained by one-dimensional ^{1}H NMR molecular modeling and a photocleavage assay. We also demonstrate that this compound induces chromosomal effects and slowing of the division of sea urchin embryos typical of G-quadruplex-interactive compounds. On the basis of molecular modeling studies, two additional analogues of this compound were designed and synthesized (QQ27 and QQ28; Fig. 1*B*), and their interactions with G-quadruplex structures and biological effects were examined. The maintenance or loss of biological potency paralleled their interactions with the G-quadruplex structure, and this was predicted on the basis of molecular modeling.

Materials and Methods

Synthesis of Extended Fluoroquinolones (QQ58, QQ27, and QQ28 in Figure 2)

General. All of the melting points were recorded on a Thomas-Hoover capillary melting point apparatus and are uncorrected. ^{1}H and ^{13}C data were obtained on a Varian Unity 300 MHz NMR spectrometer. The chemical shifts are relative to the trace proton, carbon, or fluorine signals of the deuterated solvent. Coupling constants, J, are reported in Hz and refer to apparent peak multiplicity rather than coupling constants. Mass spectroscopic experiments were performed by the Mass Spectroscopy Center at The University of Texas, Austin, TX. Elemental analysis of C, H, and N was done by Desert Analytics, Tucson, AZ. Flash column chromatography was performed on silica gel 60, 230–400 mesh, purchased from Spectrum. All of the starting materials were obtained from commercial sources unless otherwise specified.

Ethyl 3-(2-hydroxydibenzofuran-3-amino)-2-[(2,3,4,5,-tetrafluorophenyl)carbonyl] Prop-2-enoate (2). A solution of ethyl 2,3,4,5-tetrafluorobenzoylacetate (1.1 g; 4.18 mmol) in triethyl orthoformate (1 ml; 6.06 mmol) and acetic anhydride (1.8 ml; 19 mmol) was heated and stirred at 130°C for 4 h. During the process, the formed ethyl acetate was removed. The mixture was then distilled under vacuum to yield an orange oil, which was dissolved in 30 ml of dichloromethane. 3-Amino-2-hydroxydibenzofuran hydrobromide (4.07 g; 14.6 mmol), premixed with two equivalents of pyridine, was added to the dichloromethane solution, and the mixture was stirred overnight at room temperature. After the solvent was removed under reduced pressure, the remaining residue was absorbed on silica gel and subjected to flash column chromatography (ethyl acetate:hexane = 2:1), yielding a bright yellow powder (3.81 g; 83%). ^{1}H NMR ($CDCl_3$) δ (mixture of isomers; multiplet, m; singlet, s) 1.17–1.26 (m, 3H), 2.95 (s, br, 1H), 4.10–4.25 (m, 2H), 7.05–7.20 (m, 1H), 7.33 (m, 2H), 7.43 (m, 1H), 7.52 (m, 3H), 7.85 (m, 1H), 8.69 (s, 0.7H), 8.74 (s, 0.3H); ^{19}F NMR δ −156.2 (m, 1F), −154.5 (m, 0.75F), −135.4 (m, 0.25F), −140.3 (m, 0.75F), −139.4 (m, 1F), 139.3 (m, 0.25F); and MS (CI): *m/z* 474 (M + H).

Ethyl 1,2-difluoro-4-oxo-4*H*-pyrido[3,2,1-*k*,*l*]-(3-amino-2-hydroxydibenzofuranyl)[1,2-*g*]phenoxazine-5-carboxylate (3). Ethyl 3-(2-hydroxydibenzofuran-3-amino)-2-[(2,3,4,5,-tetrafluorophenyl)carbonyl] prop-2-enoate (2.32 g; 4.9 mmol) and NaH (60% in mineral oil; 0.45 g; 11.3 mmol) were mixed with freshly distilled tetrahydrofuran and stirred at −78°C for 15 min. The mixture was allowed to warm to room temperature gradually and then heated at 65°C for 30 min. The excess NaH was quenched by addition of 30 ml of methanol. The solution was evaporated to dryness, and the product was purified through flash column chromatography, yielding a yellow powder (1.84 g; 89%): mp >229°C (decomposed); ^{1}H NMR δ ($CDCl_3$) 9.01 (s, 1H), 7.90 (d, 1H, *J* = 7.8 Hz), 7.80 (dd, 1H, *J* = 7.8, 2.1 Hz), 7.39 (t, 1H, *J* = 6.9 Hz), 4.48 (q, 2H, *J* = 7.2 Hz), 1.49 (t, 3H, *J* = 7.2 Hz); ^{19}F NMR −133.6 (dd, 1F, *J* = 23, 10 Hz), −1561.5 (dd, 1F, *J* = 21, 9 Hz); and MS (CI): *m/z* 434 (M + H).

Ethyl (*R*)-1-{3-[(*tert*-butoxy)carbonylamino]pyrrolidin-1-yl}-2-fluoro-4-oxo-4*H*-pyrido[3,2,1-*k*,*l*]-(3-amino-2-hydroxydibenzofuranyl)[1,2-*g*]phenoxazine-5-carboxylate (4). Ethyl 1,2-difluoro-4-oxo-4*H*-pyrido[3,2,1-*k*,*l*](3-amino-2-hydroxydibenzofuranyl)[1,2-*g*]phenoxazine-5-carboxylate (0.232 g; 0.54 mmol) and (*R*)-3-(*tert*-butoxycarbonylamino)pyrrolidine (0.302 g; 1.62 mmol) were dissolved in 30 ml of pyridine, and the residue was purified using flash column chromatography (dichloromethane:ethylacetate = 2:3), yielding a yellow powder (0.27 g, 84%): mp: >261°C (decomposed). ^{1}H NMR δ 8.90 (s, 1H), 7.90 (d, 1H, *J* = 7.5 Hz), 7.64 (m, 3H), 7.57 (s, 1H), 7.51 (t, 1H, *J* = 6.9 Hz), 7.39 (t, 1H, *J* = 6.9 Hz), 5.35 (s, br, 1H), 4.44 (q, 2H, *J* = 7.2 Hz), 3.70 (m, 1H), 3.61 (m, 1H), 3.40 (m, 2H), 2.29 (m, 1H), 2.00 (m, 1H), 1.49 (s, 9H), 1.46 (t, 3H, *J* = 7.2 Hz); ^{19}F −119.8 (d, 1F, *J* = 13 Hz); and MS (CI): *m/z* 600 (M+1).

(*R*)-1-(3-aminopyrrolidin-1-yl)-2-difluoro-4-oxo-4*H*-pyrido[3,2,1-*k*,*l*]-(3-amino-2-hydroxydibenzofuranyl)[1,2-*g*]phenoxazine-5-carboxylic Acid HCl Salt (5; QQ58). Ethyl (*R*)-1-{3-[(*tert*-butoxy)carbonylamino]pyrrolidin-1-yl}-2-fluoro-4-oxo-4*H*-pyrido[3,2,1-*k*,*l*]-(3-amino-2-hydroxydibenzofuranyl)[1,2-*g*]phenoxazine-5-carboxylate (0.228 g; 0.526 mmol) was mixed with 10 ml of ethanol and 3 ml 1 N KOH. The mixture was refluxed for 30 min. HCl (9 ml of 2 N) and 6 ml of ethanol were then added to the mixture, and it was refluxed for 4 h. After the reaction mixture was cooled down slowly, a yellow powder was obtained by filtration, washing with water and ethanol, and drying (250 mg, 95%): mp: >250°C (decomposed); ^{1}H NMR (DMSO-d_6) 9.24 (s, 1H), 8.49 (m, 1H), 8.12 (s, 1H), 8.05 (d, 1H, *J* = 7.5 Hz), 7.69 (d, 1H, *J* = 8.4 Hz), 7.54 (t, 1H, *J* = 7.2 Hz), 7.47 (t, 1H, *J* = 13.5 Hz), 7.40 (t, 1H, *J* = 7.5 Hz), 3.80–4.05 (m, 5H), 2.31 (m, 1H), 2.08 (m, 1H); ^{19}F NMR −119.1 (d, 1F, *J* = 15 Hz); and MS (CI): *m/z* 472 (M + H). Anal. ($C_{26}H_{18}N_3FO_5$.HCl.7/4H_2O) C, H, N (Cal. C 62.09 H3.96 N8.35; Found C62.21 H3.75 N 8.13).

[10] M. A. Shammas, R. B. Batchu, J. Y. Wang, L. H. Hurley, R. J. S. Reis, and N. Munshi. Telomerase inhibition and cell growth arrest following porphyrin treatment of multiple myeloma cells, submitted for publication.

[11] The abbreviations used are: FQP, fluoroquinophenoxazine; NMR, nuclear magnetic resonance; CI, confidence interval; SA, simulated annealing; PIPER, *N,N′*-bis[2-(-1-piperidino)ethyl]-3,4,9,10-perylenetetracarboxylic diimide; PMC, primary mesenchyme cell; VP, vegetal plate.

Ethyl (*R*)-1-(3-aminopyrrolidin-1-yl)-2-fluoro-4-oxo-4*H*-pyrido[3,2,1-*k,l*]-(3-amino-2-hydroxydibenzofuranyl)[1,2-*g*]phenoxazine-5-carboxylate (6; QQ28). To a mixture of ethyl (*R*)-1-{3-[(*tert*-butoxy)carbonylamino]pyrrolidin-1-yl}-2-fluoro-4-oxo-4*H*-pyrido[3,2,1-*k,l*]-(3-amino-2-hydroxydibenzofuranyl)[1,2-*g*]phenoxazine-5-carboxylate (50 mg; 0.008 mmol) and methylene chloride (2 ml) was added trifluoroacetic acid (0.5 ml) at room temperature. After addition, the reaction mixture was stirred at room temperature for 2 h. Solvent was removed to give a residue and to this residue was added methanol (5 ml) and triethylamine (0.5 ml), and the yellow solid was collected to give a yellow powder (30 mg; 72%): mp: >210°C (decomposed); ^{1}H NMR (DMSO-d_6) δ 8.79 (s, 1H), 8.05 (s, 1H), 8.03 (s,1H), 7.81 (s, 1H), 7.61 (d, 1H, J = 8.0 Hz), 7.47 (t, 1H, J = 8.0 Hz), 7.36 (t, 1H, J = 8.0 Hz), 7.21 (d, 1H, J = 8.0 Hz), 4.23 (q, 2H, J = 6.8 Hz), 3.78 (m, 2H), 3.67 (m,1H), 3.54 (m, 2H), 2.00 (m, 1H), 1.68 (m, 1H), 1.32 (t, 3H, J = 6.8 Hz); MS (FAB): 500.6 (M + H); HRMS (FAB) calc. for $C_{28}H_{23}FN_3O_5$ 500.1622, found 500.1623; Anal. ($C_{28}H_{22}FN_3O_5.H_2O$) C, H, N (Cal. C64.98 H4.67 N8.12: Found C65.10 H4.81 N7.90).

(*R*)-1-{3-[(*tert*-butoxy)carbonylamino]pyrrolidin-1-yl}-2-fluoro-4-oxo-4*H*-pyrido[3,2,1-*k,l*]-(3-amino-2-hydroxydibenzofuranyl)[1,2-*g*]phenoxazine-5-carboxylic acid (7; QQ27). Ethyl (*R*)-1-{3-[(*tert*-butoxy)carbonylamino]pyrrolidin-1-yl}-2-fluoro-4-oxo-4*H*-pyrido[3,2,1-*k,l*]-(3-amino-2-hydroxydibenzofuranyl)[1,2-*g*]phenoxazine-5-carboxylate (100 mg; 0.17 mmol) was dissolved in methanol (6 ml), a solution of NaOH (37 mg; 0.67 mmol) in water (3 ml) was added, and the reaction mixture was stirred at room temperature for 2 h. Methanol was evaporated off, clear solution was neutralized with 10% HCl to pH = 2.0, and precipitate was collected and dried with a vacuum pump to give a yellow powder (91 mg, 95%): MP: 235–237°C; ^{1}H NMR (DMSO-d_6) δ 9.15 (s, 1H), 8.40 (s,1H), 8.04 (d, 1H, J = 7.5 Hz), 7.94 (s, 1H), 7.66 (d, 1H, J = 8.2 Hz), 7.51 (t, 1H, J = 7.5 Hz), 7.39 (m, 2H), 4.12 (m, 1H), 3.95 (m, 1H), 3.89 (m, 1H), 3.77 (m, 1H), 3.56 (m, 1H), 2.11 (m,1H), 1.89 (m, 1H),1.41 (m,1H); MS (FAB): 572.6 (M + H); HRMS (FAB) (M + H) calc. for $C_{31}H_{27}FN_3O_7$ 572.1838, found 572.3338; Anal. ($C_{31}H_{26}FN_3O_7.7/4H_2O$) C, H, N (Cal. C61.73 H4.63 N7.13; Found C61.97 H4.50 N6.96).

Drug and Oligonucleotide Preparation. Drug solutions were prepared as 5 mM stock solutions in DMSO and stored at −20°C. These stock solutions were diluted to working concentrations in distilled water immediately before use. Oligonucleotides were synthesized on a PerSeptive Biosystems Expedite 8909 automatic DNA synthesizer. The samples for NMR experiments were purified by reverse phase high-performance liquid chromatography on a C18 column (Dynamax-300A) and dialyzed extensively against 10 mM KCl or 20 mM NaCl solutions followed by deionized water. Solid supports and phosphoramadites were purchased from Glen Research and PerSeptive Biosystems. Oligonucleotides for polymerase extension assay and photocleavage reactions were purified by denaturing PAGE, diluted to required concentrations, and dispensed into small aliquots.

Decatenation Assay. Kinetoplast DNA (0.25 μg) was incubated with various concentrations of QQ58 or A-62176 in 10 μl of reaction buffer [50 mM Tris-HCl (pH 8.0), 120 mM KCl, 10 mM $MgCl_2$, 0.5 mM ATP, and 0.5 mM DTT) for 10 min. Two units of human topoisomerase II (TopoGEN Inc.) were added to the mixture, which was then incubated at 37°C for 30 min. The reaction was terminated with 0.1 volume of stop buffer (5% sarkosyl, 0.025% bromophenol blue, and 50% glycerol). The decatenation products were analyzed on 1% agarose gels run with 0.5 μg/ml ethidium bromide.

Preparation and End-labeling of Oligonucleotides for Topoisomerase II Cleavage Reaction. DNA oligomers 5′-d[CGATGGGGAAGATCGGGCTCGTATACATTGATACGGGGCTCATGAGCGCTTGTTTCGGCG]-3′ (A1) and 5′-d[CGCCGAAACAAGCGCTCATGAGCCCCGTATCAATGTATACGAGCCCGATCTTCCCCATCG]-3′ (A2; Ref. 46) were synthesized as above. The 5′ end-labeled single-strand oligonucleotide was obtained by incubating A1 with T4 polynucleotide kinase and [γ-^{32}P]ATP at 37°C for 1 h. Labeled DNA was purified with a Bio-Spin 6 chromatography column (Bio-Rad) after inactivating T4 polynucleotide kinase by heating for 8 min at 70°C. The labeled strand was then annealed with the complementary strand (A2) and purified on an 8% native polyacrylamide gel.

Topoisomerase II Cleavage Reaction. The labeled double-stranded DNA was incubated with 20 units of human topoisomerase II in 20 μl of reaction buffer [30 mM Tris-HCl (pH 7.6), 3 mM ATP, 15 mM β-mercaptoethanol, 8 mM $MgCl_2$, and 60 mM NaCl] at 30°C for 10 min in the presence of various concentrations of QQ58 or A-62176. Reactions were terminated by adding SDS to 1% of the final concentration, and topoisomerase II was removed by proteinase K digestion (100 μg/ml) at 42°C for 1 h followed by phenol-chloroform extraction and ethanol precipitation. Samples were loaded onto a 12% denaturing sequencing gel. The dried gels were exposed on a phosphor screen. Imaging and quantification were performed using a PhosphorImager (Storm 820) and ImageQuant 5.1 software from Molecular Dynamics.

Telomerase Assay. Telomerase assays were run as described previously (47) using a primer extension assay in which a 5′-biotinylated primer consisting of three telomeric repeats was used, and the incorporation of ^{32}P-labeled GTP was measured. In brief, reaction mixtures (20 μl) contained 4 μl of cell extracts (60 μg total cell protein), 50 mM Tris-OAc (pH 8.5), 50 mM K-OAc, 1 mM $MgCl_2$, 5 mM BME, 1 mM spermidine, 1 μM 5′-biotinylated telomere primer $(TTAGGG)_3$, 1.2 μM [α-^{32}P]-dGTP (800 Ci/mmol), 1 mM dATP, and 1 mM dTTP, and were incubated at 37°C for 30 min. Reactions were terminated by adding 20 μl of Streptavidin-Dynabeads, which bind selectively to the desired targets (5′-biotinylated primer), forming a magnetic bead-target complex. This complex was separated from the suspension using a magnet (Dynal MPC) and washed several times with washing buffer (2 M NaCl) to eliminate [α-^{32}P]-dGTP background. Telomerase reaction products were separated from the magnetic beads by protein denaturation with 5.0 M guanidine-HCl at 90°C for 30 min. After recovery of these products, analysis was performed by 8% denaturing PAGE. Telomerase activities were quantified by densitometric analyses of an autoradiogram using ImageQuant software.

All of the reactions were carried out in amber Eppendorf tubes under subdued lighting to avoid photocleavage.

Polymerase Stop Assay. The DNA primer 5′-d[TAATACGACTCACTATAG]-3′ and template DNA 5′-d[TCCAACTATGTATAC(TTGGGG)$_4$TTAGCGGCACGCAATTGCTATAGTGAGTCGTATTA]-3′ were synthesized and purified as before (48). About 200 ng of the primer DNA was 5′-end-labeled with ^{32}P using T4 polynucleotide kinase and subsequently purified by denaturing PAGE. The assay was carried out as described previously (48). Briefly, 24 nM of labeled primer and 12 nM of template DNA were annealed in a 1 × reaction buffer [10 mM Tris-HCl (pH 8.0) and 5 mM KCl] by heating to 95°C and slowly cooled to room temperature. $MgCl_2$, dNTP, and Taq DNA polymerase (Boeringher-Manheim) were added, and the mixture was incubated at 55°C for 20 min. The polymerase extension was stopped by adding 2 × stop buffer (10 mM EDTA, 10 mM NaOH, 0.1% xylene cyanol, and 0.1% bromphenol blue) and loaded onto a 12% sequencing gel. After electrophoresis, the gels were dried and visualized on a PhosophorImager and quantitated using ImageQuant software.

Photo-mediated Strand Cleavage Reaction. The sequence of the single-stranded DNA (G-quadruplex) used was 5′-d[CATGGTGGTTT(GGGTTA)$_4$CCAC]-3′. About 400 ng of G-quadruplex DNA was 5′-end-labeled with ^{32}P using T4 polynucleotide kinase (New England Biolabs) and subsequently purified by denaturing PAGE. This 5′-labeled G-quadruplex DNA was stored in Tris-EDTA buffer [10 mM Tris-HCl, 1 mM EDTA (pH 7.5)] at a concentration of 5 ng/μl and ~3000 cpm/μl. For each photocleavage reaction, 30 μl of G-quadruplex DNA was mixed with 30 μl of a 200 mM KCl solution, placed in a water bath at 95°C for 4 min, and slowly cooled to room temperature. A control set was run in distilled water instead of KCl solution. QQ58 (6 μl) at varied concentrations was added to each sample and transferred to a 24-well Titretek microtiter plate (ICN). This plate was placed on top of a Pyrex glass shield and irradiated for 2 h with an 85-W xenon lamp placed under the Pyrex glass. (Pyrex glass was used to filter the UV light under 300 nm, thereby eliminating DNA damage caused directly by UV irradiation.) During the irradiation, the Titretek plate was rotated three times to eliminate light heterogeneity. Reactions were terminated by the addition of 10 μg of calf thymus DNA, followed by phenol-chloroform extraction and ethanol precipitation. The resulting samples were subjected to treatment with 0.1 M piperidine. The samples were then loaded onto a 16% sequencing gel and electrophoresed. The dried gels were exposed to a phosphor screen. Imaging and quantification were performed using a PhosophorImager and ImageQuant software.

NMR Spectroscopy. NMR experiments were performed on a Varian UNITY plus 500 MHz spectrometer. All of the titration experiments were carried out at 30°C in a 90% H_2O/10% D_2O solution containing 150 mM KCl, 25 mM KH_2PO_4, and 1 mM EDTA (pH 7.0). A standard 1–1 echo pulse sequence with a maximum excitation centered at 12 ppm was used for water suppression. Thirty-two scans were acquired for each spectrum with a relaxation delay of 2 s. Two-dimensional Nuclear Overhauser Effect Spectroscopy spectra of exchangeable protons were collected at 30°C in time proportional phase incrementation mode with a mixing time of 200 ms using 2048 and 1024 complex points in t_2 and t_1 experiments, respectively. NMR data were processed and analyzed using the FELIX program (Molecular Simulations Inc.). Nearly all of the nonexchangeable DNA protons of the 5′-d[A(G_3T_2A)$_3G_3$]-3′ and 5′-d[TAG_3T_2A]$_4$-3′ in a free form or in a complex with ligand, except for several H5′/H5″ pairs, were assigned as described (49).

Model Building and Molecular Dynamics Simulations. The initial coordinates used in the model building process were those published for the NMR-based model of the 1:1 PIPER:5′-d[TAG_3T_2A]$_4$-3′ complex (49) and the antiparallel human telomeric sequence d[$AG_3(T_2AG_3)_3$] (50). The necessary replacements and the addition of hydrogens were carried out using INSIGHT II (Ref. 51; Molecular Simulations Inc.), and position was refined by energy minimization (1000 cycles of steepest descent and 2 × 1000 cycles of conjugate gradient) while constraining the positions of heavy atoms. Finally, the entire structure was subjected to conjugate gradient minimization until convergence was reached, at which time constraints were gradually removed. Molecular dynamics simulations (100 ps) at 300 K and mechanics (2 × 1000 cycles of conjugate gradient minimization) were performed using DISCOVER with the consistent force field. This structure subsequently served as the starting structure for additional energy refinement, docking, molecular dynamics, and complex formation.

To explore the molecular interactions of QQ58 and its analogues, QQ27 and QQ28, with the G-quadruplex structures, molecular models were built and energy minimized using a protocol similar to that described for G-quadruplex structures. The obtained low energy structures were manually docked into the intercalation site, and energies were computed using the AFFINITY (52) program. To clarify the orientation of the ligands in the intercalation site, the electrostatic potentials at the van der Waals surface of the G-quadruplex were determined by using solvent surface calculations. The SA docking with 100 fs/stage duration (50 SA stages) was then performed to find the most favorable orientation. Thus, orientation with low intermolecular potential energy was obtained while moving ligand and ligand-binding G-tetrad residues. The resulting ligand-G-quadruplex complex trajectories were energy minimized using 1000 cycles of conjugate gradient minimizer, and the interaction energies were computed.

Cytotoxicity Assay. Human breast carcinoma MDA-MB-231 and prostate carcinoma DU-145 cell lines were purchased from American Tissue Culture Collection (Rockville, MD) and cultured according to the supplier's instructions. Exponentially growing cells (1–2 × 10^3 cells) in 0.1 ml of medium were seeded on day 0 in a 96-well microtiter plate. On day 1, 0.1-ml aliquots of medium containing graded concentrations of the investigational compound were added to the cell plates. At days 7–10, the cell cultures were incubated with 50 μl of 3-(4,5-dimethylthiazol-2-yl)-2,5-diphenyltetrazolium bromide (1 mg/ml in Dulbecco's PBS) for 4 h at 37°C. The resulting formazan precipitate was solubilized with 200 μl of 0.04 M HCl in isopropyl alcohol (53). For determi-

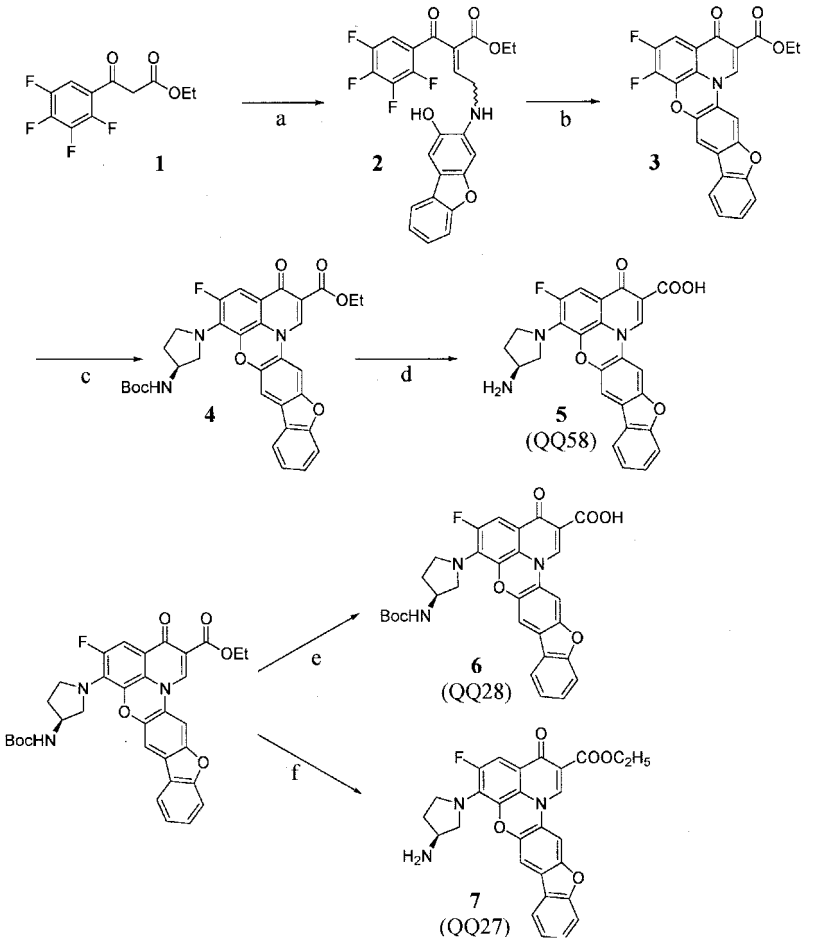

Fig. 2. Condition: (a) (i) Ac_2O, $CH(OC_2H_5)3$, (ii) 3-amino-4-hydroxydibenzofuran hydrobromide; (b) THF, NaH; (c) pyridine, (R) t-Boc-3-aminopyrrolidine; (d) OH^-/H^+; (e) OH^-; (f) CF_3COOH.

nation of the IC_{50} values, the absorbance readings at 570 nm were fitted to the four-parameter logistic equation.

Sea Urchin Embryo Culture. *Lytechinus pictus* sea urchins (Marinus Inc., Long Beach, CA) were maintained at 15°C in refrigerated aquaria containing Instant Ocean artificial sea water. Spawning, fertilization, drug treatment, and embryo processing were done as described (54). Briefly, 10 min after insemination, the fertilized eggs were allowed to settle, and the supernatant was aspirated and replaced with fresh artificial sea water. The embryos were cultured at 18°C. Stock solutions (10 mM) of the tested agents were prepared in DMSO. Twenty min after fertilization, the agents were added to 1% embryo suspensions to a final concentration of 1 μM. Equivalent amounts of DMSO were added to control egg suspensions. At measured times after insemination (10 and 24 h), the embryos were pelleted by centrifugation. Video images of the embryos were captured with a Zeiss standard research microscope interfaced with a Javelyn video camera and a Panasonic time-lapse video recorder. The nuclei were stained by the Feulgen reaction, and the chromatin was visualized and photographed with an Olympus BH2 photomicroscope equipped with fluorescence optics, as described elsewhere (55).

Results

Chemistry. The synthetic procedure (Fig. 2) was based on a published method for the synthesis of the quinobenzoxazines, with some modification (56). The synthesis was started with ethyl 2,3,4,5-tetrafluorobenzoylacetate (Fig. 2, *1*), which was prepared according to published procedure (5). Treatment of 2,3,4,5-tetrafluorobenzoylacetate with triethyl orthoformate in acetic anhydride followed by 2-hydroxy-3-amino-dibenzofuran hydrobromide generated the enamino keto acid intermediate (Fig. 2, *2*). This intermediate was treated with sodium hydride at −78°C and then heated to reflux to complete the double annulation (Fig. 2, *3*). Regioselective nucleophilic substitution of fluoride with 3-(*R*)-(*tert*-butoxycarbonylamino)pyrrolidine was carried out to give the key intermediate (Fig. 2, *4*). Final target molecules *5*, *6*, and *7* (Fig. 2) were prepared by hydrolysis and deprotection of *4*, hydrolysis of *4*, and deprotection of *4*, respectively, in overall yields of 59, 59, and 44.7%, respectively.

Comparison of the Effects of A-62176 and QQ58 on Topoisomerase II and Telomerase Activity

On the basis of our previous insights into structural requirements (extended planarity, cationic interactions) for ligand binding with G-quadruplex structures, the fluoro-

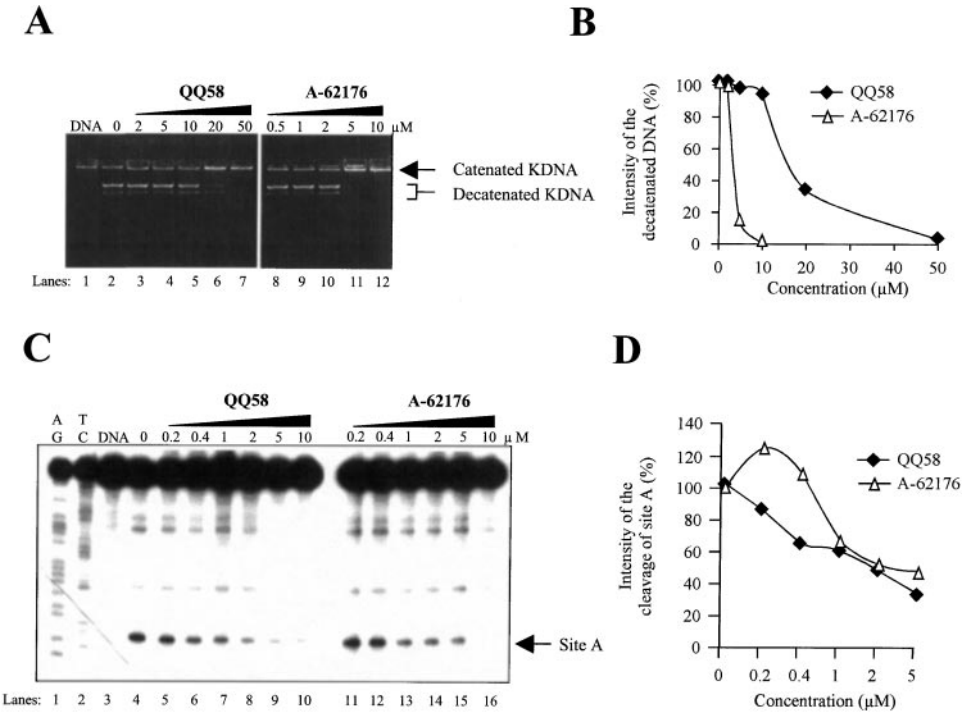

Fig. 3. *A,* inhibition of decatenation of human topoisomerase II by QQ58 and A-62176. Catenated KDNA was treated with 2 units of human topoisomerase II in the presence of QQ58 or A-62176 followed by SDS/proteinase K and then analyzed on agarose gel. *Lane 1* contains catenated KDNA only. *Lane 2* contains KDNA and topoisomerase II without compounds. *Lanes 3–7* contain 2, 5, 10, 20, and 50 μM of QQ58, respectively. *Lanes 8–12* contain 0.5, 1, 2, 5, and 10 μM of A-62176, respectively. *B,* intensity of decatenated KDNA was quantitated from the gel using ImageQuant software. *C,* autoradiogram of a 12% denaturing polyacrylamide gel showing the topoisomerase II-mediated cleavage pattern in the presence of QQ58 or A-62176. The cleavage reaction was done in a reaction buffer as described in "Materials and Methods." *Lane 3* contains DNA only. *Lane 4* contains DNA and topoisomerase II without QQ58 or A-62176. *Lanes 5–10* and *11–16* contain 0.2, 0.4, 1, 2, 5, and 10 μM QQ58 and A-62176, respectively. *D,* strand breakage products indicated by the *arrow* in *C* were quantitated using a PhosphorImager and ImageQuant software. The intensity of the DNA cleavage produced by QQ58 or A-62176 was determined from the volume of the bands normalized by the total radioactivity in each lane.

quinolones seemed to be good candidates for structural modification. Our objective was to convert a topoisomerase II poison (A-62176) to a G-quadruplex-interactive compound. As this work progressed, a paper was published (4) that demonstrated that quinolones were telomerase inhibitors, suggesting to us that quinolones might interact with G-quadruplex structures. Our first objective was to compare the topoisomerase II inhibitory activities and G-quadruplex interactions of A-62176 and QQ58 to determine whether it would be possible to separate these activities.

Whereas A-62176 Is Both a Topoisomerase II Poison and a Catalytic Inhibitor, QQ58 Is Only a Catalytic Inhibitor. Experiments were designed to compare the effects of A-62176 and QQ58 on the activity of human topoisomerase II. The ability to cleave and religate double-stranded DNA is central to the physiological functions of topoisomerase II. Kinetoplast DNA is a massive network consisting of thousands of interlocked, closed circular DNA molecules called minicircles. Topoisomerase II introduces a double-strand break in DNA to release one minicircle from the network, which is called a decatenation reaction (57, 58). The *in vitro* effects of A-62176 and QQ58 were determined by using a decatenation assay. As shown in Fig. 3, *A* and *B,* QQ58 had about a 5-fold lower decatenation activity than A-62176. To additionally characterize the properties of A-62176 and QQ58, the contrasting effect on the DNA cleavage reaction of human topoisomerase II of QQ58 was determined. As shown in Fig. 3, *C* and *D,* the intensity of the topoisomerase II-mediated cleavage at site A decreased as the concentration of QQ58 was increased, whereas the DNA cleavage was initially enhanced at low concentrations of A-62176 and then decreased at high concentrations. These results show that the two fluoroquinolones act differently on human topoisomerase II: QQ58 acts as a catalytic inhibitor that inhibits the activity of topoisomerase II without trapping the cleaved complex, and A-62176 is a topoisomerase II poison that interferes with the breakage-rejoining reactions of topoisomerase II by trapping the enzyme covalent reaction intermediate, known as the cleaved complex.

QQ58 Is a More Potent Inhibitor of Telomerase than A-62176, but Is Less Potent than the Cationic Porphyrin TMPyP4. The telomerase inhibitory activity of QQ58 was compared with A-62176 and the cationic porphyrin TMPyP4 (Fig. 1*B*), a known inhibitor of telomerase because of its ability to sequester the single-stranded DNA primer required for the reverse transcriptase activity of telomerase into a G-quadruplex structure (Ref. 6, 59; Fig. 4*A*). The IC_{50} values for the inhibition of telomerase assay in the direct assay for A-62176, QQ58, and TMPyP4 were 58, 28, and 8 μM, respectively. These were determined from the histogram plots shown in Fig. 4*B*. It is important to note that the telomerase

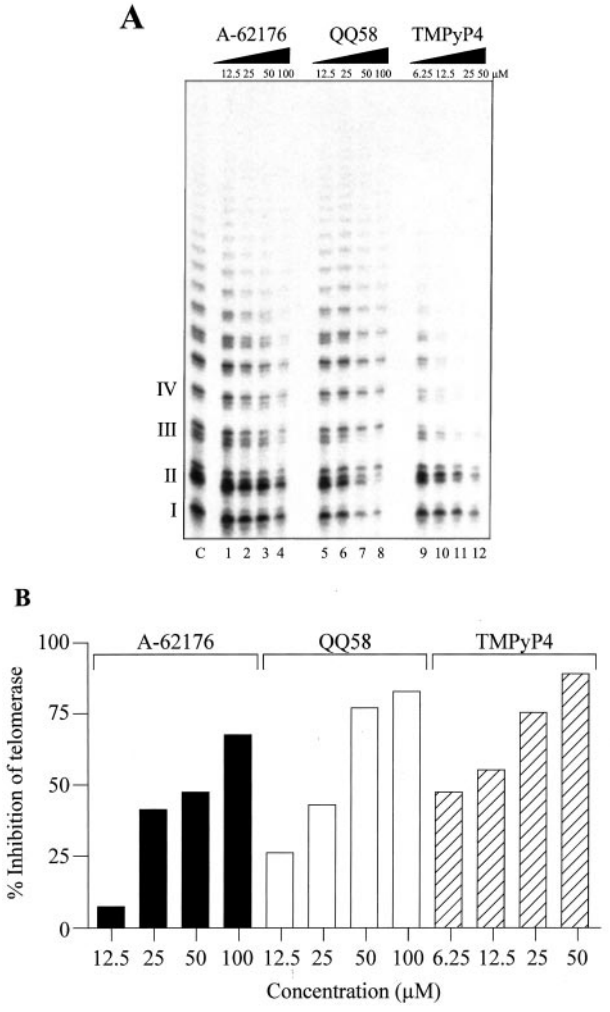

Fig. 4. Inhibition of human telomerase by A-62176, QQ58, and TMPyP4. *A,* autoradiogram showing telomerase inhibition with increasing concentrations of A-62176, QQ58, and TMPyP4. *Lanes 1–4*, *5–8,* and *9–12* contain 12.5, 25, 50, and 100 μM of A-62176, QQ58, and TMPyP4, respectively. *B,* graphical representation of data from *A*.

inhibitory potencies are ~10-fold less than in the more familiar PCR-based telomeric repeat amplification protocol assay. Thus, by extension of the quinobenzoxazine fused ring system of A-62176 (Fig. 1*B*) to the quinophenoxazine ring system in QQ58 (Fig. 1*B*), QQ58 shows an ~2-fold increase in potency in inhibition of telomerase over A-62176, but this is still less than TMPyP4.

Physical and Biochemical Characterization of the Interaction of QQ58 with the Intramolecular Antiparallel and Intermolecular Parallel G-Quadruplex Structures

QQ58 Stabilizes an Intramolecular G-Quadruplex Sufficiently to Cause Polymerase Pausing. The polymerase stop assay (48) can be used to evaluate the interaction of ligands with the intramolecular G-quadruplex structures. The principle of this assay is shown in the cartoon in Fig. 5*A*. This assay was originally developed to study the effect of G-quadruplex secondary structures on polymerase processivity (60). It has also been adopted to aid in the identification of the compounds that bind to and stabilize G-quadruplex structures (48). QQ58 causes a sequence-specific inhibition of Taq polymerase at the G-quadruplex site on the template DNA (Fig. 5*B*). As expected, there is polymerase pausing as the enzyme extends primer along the template, even in the absence of QQ58 in lane 1 of Fig. 5*B* (attributable to the presence of potassium in the reaction buffer that facilitates G-quadruplex formation). However, as the concentration of QQ58 is increased, there is enhanced pausing at the G-quadruplex site on the template DNA (Fig. 5*B*). The ratio of the intensity of the bands at the G-quadruplex pause site to the total intensity per lane increases by ~3-fold as the concentration of QQ58 increases from 0 to 10 μM (Fig. 5*C*). This indicates that QQ58 interacts with the G-quadruplex sufficiently to stabilize the G-quadruplex structure and inhibit the polymerase stop assay. In this same assay, A-62176 had little effect on the pausing of Taq polymerase at the G-quadruplex structure site.[12]

^{1}H NMR Studies Demonstrate That QQ58 Forms a Stable Complex with a Parallel-stranded G-Quadruplex in Which the Drug Stacks at the GT Step. We chose the $d[TAG_3T_2A]_4$ intermolecular G-quadruplex ("b" in Fig. 1*A*) for these studies on the basis of its relevance to the human telomeric TTAGGG repeat and our previous success in determining the solution NMR structure of its complex with another telomerase inhibitor (49). The one-dimensional ^{1}H NMR spectra recorded during the titration of $d[TAG_3T_2A]_4$ with QQ58 are shown in Fig. 6*A*. The ^{1}H NMR signals of the Hoogsteen-bound guanine imino protons (10–12 ppm range) gradually disappeared during the titration, and a new set of reciprocal upfield-shifted broadened imino proton resonances appeared, as shown at the QQ58:DNA ratio of 1:1 (Fig. 6*A*). The more pronounced upfield shift of the G5 imino proton relative to G4 and G3 infers that the site of QQ58 binding is between G5 and T6. Separate proton resonances for the free DNA and the drug:G-quadruplex DNA complex point to the slow exchange rate on the NMR time scale between the free and bound DNA. The spectra are very comparable with the spectra that were obtained for the titration of PIPER with the same oligonucleotide (49). These NMR results indicate a strong and specific binding of QQ58 with parallel G-quadruplex DNA. Although attempts to obtain a two-dimensional NOESY spectra were made, the quality of the spectra impaired spectral assignment. The drug proton resonances were difficult to assign despite the complete assignment of the protons of the G-quadruplex in both the unbound and drug-bound states. Nevertheless, the identical changes in the DNA spectra on titration with either QQ58 or PIPER argue for a common geometry of the drug-G-quadruplex complexes. Because the structure of the PIPER-G-quadruplex complex has already been determined (49), it was used as a reference point for additional molecular modeling studies. A proposed model of the QQ58-intermolecular

[12] A. Rangan, unpublished observations.

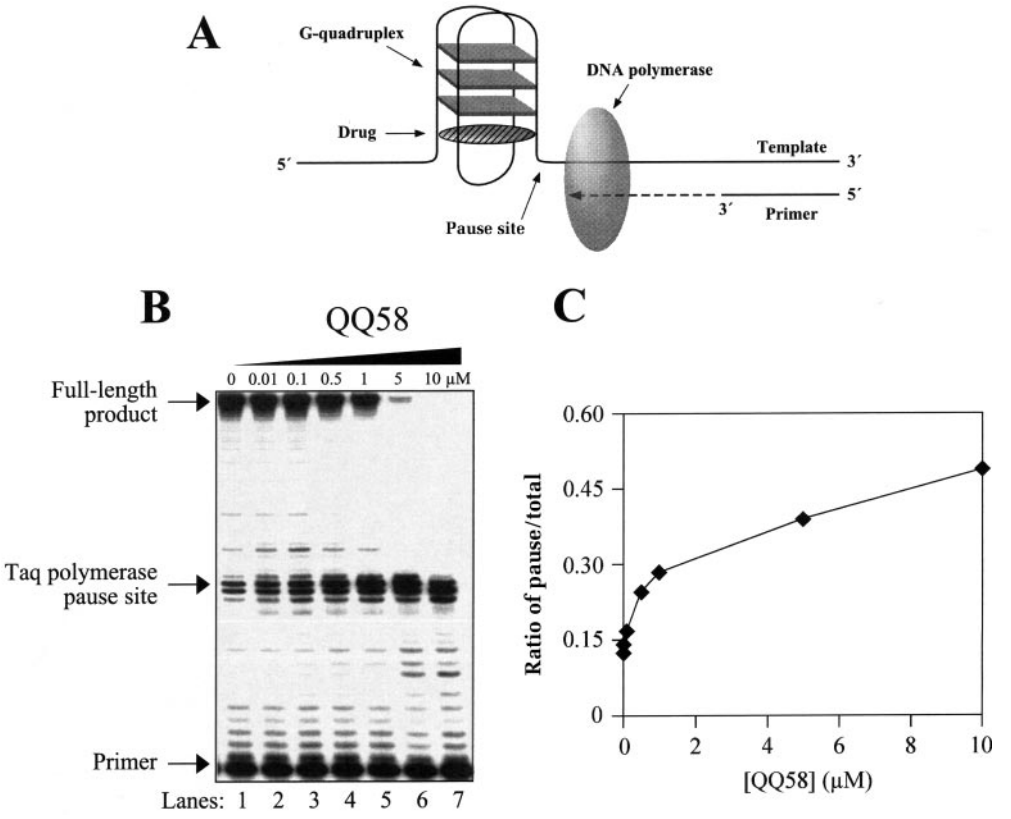

Fig. 5. Inhibition of Taq polymerase with increasing concentrations of QQ58. *A,* cartoon of the assay. *B,* autoradiogram of the sequencing gel showing enhanced DNA synthesis pausing at the G-quadruplex site with increasing concentrations of QQ58 *(Lanes 1–7)*. The free primer, the pause site, and the full-length product are indicated. *C,* graphical representation of the quantification of the sequencing gel shown in *B,* showing the concentration of QQ58 to the ratio of intensity of the bands obtained for the pausing site/total intensity per lane.

four-stranded G-quadruplex complex was prepared.[13] The drug molecule binds to the G-quadruplex at the GT step by stacking of the aromatic moiety to the surface of the 3′-terminal G-tetrad. The binding site and QQ58 molecule orientation in regard to DNA bases are identical to those of the PIPER-G-quadruplex complex. This explains the similarity in the pattern of the chemical shift changes.

QQ58 Binds to the Intramolecular G-Quadruplex Structure by Stacking between the Diagonal Loop and External G-Tetrad. The intramolecular basket conformation of a monomeric G-quadruplex DNA ("d" in Fig. 1*A*) is likely to be involved in the interaction with proteins and ligands *in vivo* (38). To examine the interaction of QQ58 with the intramolecular G-quadruplex structure, ^{1}H NMR studies were carried out, with the established basket G-quadruplex consisting of the 22-mer human telomeric sequence d[$AG_3(T_2AG_3)_3$] (50). The one-dimensional NMR titration of 22-mer DNA with QQ58 is shown in Fig. 6*B*. The spectra of the imino protons in the region of 10–12 ppm demonstrate the shift of only one particular Hoogsteen bped guanine, namely, the G22 residue that is a part of the G-tetrad adjacent to the diagonal loop. This suggests that the interaction of QQ58 with intramolecular G-quadruplex is in the proximity of this G-tetrad. The complexity of the one-dimensional spectra in the imino proton region, arising because of either strand aggregation or dynamics within the NMR time scale used, made the interpretation of the two-dimensional NOESY spectra rather complex. Thus, to additionally characterize the intramolecular QQ58-G-quadruplex complex, photocleavage studies were performed.

Photo-mediated DNA Cleavage Reactions Confirm the Proximity of QQ58 to the External G-Tetrad. To additionally characterize the binding mode of QQ58 to the intramolecular G-quadruplex structures, a photo-mediated cleavage reaction of the QQ58-G-quadruplex complex was carried out. A DNA sequence that forms an intramolecular G-quadruplex under conditions standardized previously was used (12). The photo-reactive property of the FQPs leads to strand cleavage in the QQ58-G-quadruplex complex in the presence of light of a specific wavelength. This in turn gives important information about the drug localization in the complex. The photocleavage pattern produced by QQ58 on the intramolecular G-quadruplex is shown in Fig. 7*A*. With increased concentrations of the drug, there is enhanced cleavage at G1, G6, and G12, which correspond to specific guanines involved in the G-quadruplex. These guanines, G1, G6, and G12, correspond to the residues that form the lowermost G-tetrad (Fig. 7*B*), with G12 and G6 being the most reactive residues. This photocleavage data confirms that the drug is bound external to this G-tetrad. On the basis of the NMR studies and the photocleavage experiments, a cartoon (Fig. 7*B*) is proposed for the binding of QQ58 with the sequence that forms an intramolecular G-quadruplex structure (Ref. 12; Fig. 7*B*). G12 in this structure corresponds to G22 in the previous two-dimensional ^{1}H NMR study, providing con-

[13] O. Fedoroff, unpublished observations.

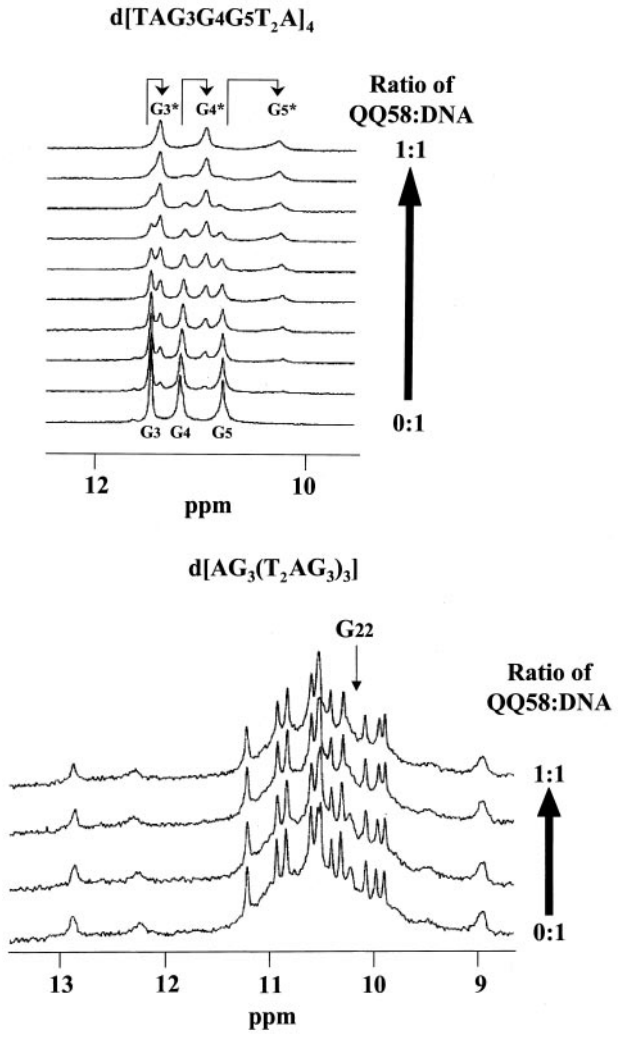

Fig. 6. Effect of QQ58 on the ^{1}H NMR spectra of G-quadruplex structures. *A,* one-dimensional ^{1}H NMR titration of d[$TAG_3T_2A]_4$ with QQ58 to obtain a 1:1 QQ58:DNA ratio. The imino proton and aromatic proton regions of the 500 MHz NMR spectra are shown with increasing amounts of ligand added at 30°C. G3, G4, and G5 represent the imino proton resonances of the free DNA, whereas G3*, G4*, and G5* represent the imino proton resonances of the ligand-bound DNA. *B,* one-dimensional ^{1}H NMR titration of d[$AG_3(T_2AG_3)_3$] with QQ58 to obtain a 1:1 QQ58:DNA ratio. The imino proton regions of the 500 MHz NMR spectra are shown with increasing amounts of ligand added at 30°C. The *arrow* points to the imino proton resonance of G22, which shifts on addition of QQ58.

firmation of the location of QQ58 in the intramolecular fold-over G-quadruplex structure.

Molecular Modeling Predicts That QQ58 Binds to the Human Intramolecular Telomeric Repeat d[$AG_3(T_2AG_3)_3$]. Docking simulations and analysis revealed that QQ58 binds to the human intramolecular telomeric repeat d[$AG_3(T_2AG_3)_3$] G-quadruplex with a binding energy of −75.6 kcal/mol (Table 1*A*). Although this binding energy is lower than that of QQ58 with the parallel-stranded G-tetraplex (see later), the favorable interactions in the T_2A loop suggest that it is a human telomeric G-quadruplex-interactive agent. The aminopyrrolidine-NH_2 is oriented to interact with G10 within the proposed intercalation site. Furthermore, the central ring nitrogen is positioned into the guanine carbonyl channel, and the carboxylic acid functional group extends into the minor groove. The extended phenoxazine ring exhibits stacking interactions with the G14 and G10 bases. This orientation was confirmed as the most stable docking model by binding energy calculations.

Comparison of the Biochemical and Biological Effects of QQ58 and Its Amino (QQ27) and Carboxyl-modified (QQ28) Analogues

On the basis of NMR and photocleavage data, initial molecular modeling results suggested a complex in which QQ58 stacks to the external tetrad in both the intramolecular antiparallel and parallel G-quadruplex structures, as illustrated for the former in Fig. 7*B*. Molecular modeling was carried out on the human telomeric antiparallel (Fig. 8*A*) and parallel-stranded (Fig. 8*B*) G-quadruplex structures with QQ58 to gain additional insight into these structures, and on the basis of the results from the parallel-stranded G-quadruplex, two synthetically accessible molecules (QQ27 and QQ28 in Fig. 1*B*) were designed and synthesized, which were predicted to effect specific H-bonding interactions between the FQP and the G-quadruplex structures, resulting in much less favorable interactions of QQ28 with the intermolecular parallel-stranded G-quadruplex structure than either QQ27 or QQ58. A parallel series of biochemical and biological experiments were carried out to test these ideas.

Molecular Modeling Predicts That QQ58 Has a Higher Binding Interaction with the G-Quadruplex Structure. Molecular modeling and SA docking experiments revealed that QQ58 exhibited the highest binding interactions with the four-stranded parallel G-quadruplex (d[$TAG_3T_2A]_4$; Table 1*B*) and is intercalated at the G5-T6 nucleotide step approximately between two pairs of guanines and thymines, with the positively charged side chain located in the groove (Fig. 8*B*). A strong intermolecular hydrogen bond interaction of the N7 atom of G5 with the carboxylic proton of QQ58 (N7 to COOH is 2.38 Å) was observed (Fig. 8*C*). The QQ58 aminopyrrolidine amino group takes part in a hydrogen bonding interaction with the 5′ phosphate group of G5 (Fig. 8*C*). QQ58 also shows favorable stacking interactions between the G5 guanine tetrad and two of the 6-thymine residues. These electrostatic (−167.5 Kcal/mol) and van der Waals (−96.4 Kcal/mol) interactions give rise to a calculated binding energy of −86.4 Kcal/mol (Table 1*B*). In the case of compound QQ28, such interactions were not observed, presumably because of the strong steric clash of the *tert*-butoxy carbonyl group of the aminopyrrolidine with G5 at the intercalation site. This in turn leads to the shift of the carboxylic acid functionality from its H-bonding site at G5. Analysis of all of the dynamic trajectories reveals that the *tert*-butoxy carbonyl group is rigidly positioned and oriented. This results in dramatic loss of both electrostatic and van der Waals energies relative to QQ58. Similarly, the presence of an ethyl ester group in the case of QQ27 restricts the electrostatic and hydrogen bonding interactions with the G5 nucleotide region of the intercalation site but to a much lesser extent than in QQ58. The calculated binding energies for QQ27 and QQ28 with the parallel-stranded complexes are −26.5 and 112.6 Kcal/mol, respectively.

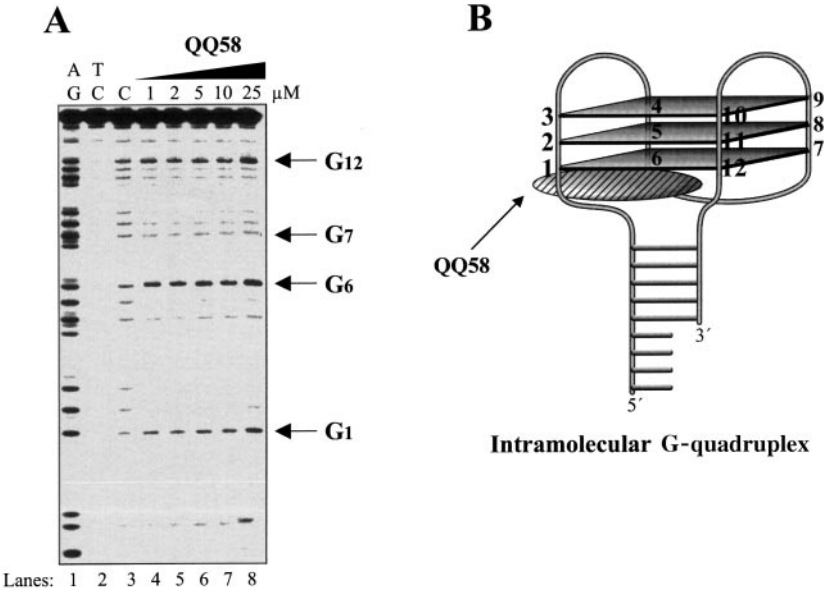

Fig. 7. QQ58 photo-mediated strand cleavage reaction of intramolecular G-quadruplex. *A,* autoradiogram of a photocleavage sequencing gel with increasing concentrations of QQ58. *Lanes 1* and *2* are the AG/TC Maxam-Gilbert sequencing reactions, and *Lanes 4–8* are increasing concentrations of QQ58 (1–25 μM). The enhanced cleavage sites are indicated by G1, G6, and G12. G7 is in the same tetrad but is not cleaved excessively. *B,* diagrammatic representation of the proposed external binding of QQ58 to the G-quadruplex below the lower-most G-tetrad based on the photocleavage results with the ligand.

Table 1 Computed interaction energies (kcal/mol)

A. Energies for QQ58 human telomeric repeat d[$AG_3(T_2AG_3)_3$] G-quadruplex

Ligand	d[$TAG_3T_2A]_4$-ligand VdW energy	d[$TAG_3T_2A]_4$-ligand electrostatic energy	d[$TAG_3T_2A]_4$-ligand total energy	Ligand VdW energy	Ligand electrostatic energy	Ligand total energy	Calculated binding energy
QQ58	−62.7	−176.1	−238.8	−78.9	−84.3	−163.2	−75.6

B. Energies (kcal/mol) for QQ58-, QQ28-, and QQ27-parallel-stranded G-quadruplex (d[$TAG_3T_2A]_4$) complexes

Ligand	d[$TAG_3T_2A]_4$-ligand VdW energy	d[$TAG_3T_2A]_4$-ligand electrostatic energy	d[$TAG_3T_2A]_4$-ligand total energy	Ligand VdW energy	Ligand electrostatic energy	Ligand total energy	Calculated binding energy
QQ58	−96.4	−167.5	−263.9	−61.3	−116.2	−177.5	−86.4
QQ28	89.2	253.4	342.6	92.5	137.5	230.0	112.6
QQ27	−116.1	−178.1	−294.2	−69.3	−198.4	−267.7	−26.5

The Polymerase Stop Assay Demonstrates That QQ28 Has Only a Minimal Stabilizing Effect on G-Quadruplex Structure, Whereas QQ27 Has an Intermediate Effect. On the basis of molecular modeling results, we predicted that the steric bulk of the N-Boc group on the aminopyrrolidine of QQ28 should interfere with intercalation into the G-quadruplex structure and prevent any ionic interaction between the positively charged amino group of QQ28 and the anionic backbone of DNA. However, the ethyl ester of QQ58 should not dramatically affect the binding of QQ27. A polymerase stop assay was used to evaluate the comparative abilities of QQ58, QQ27, and QQ28 to stabilize the intramolecular fold-over G-quadruplex structure. The results shown in Fig. 9, *A* and *B,* demonstrate that, as predicted, QQ58 and QQ27 have approximately the same potency in inhibition of the Taq polymerase, whereas QQ28 was much less potent.

Comparative Cytotoxicity Measurements of QQ58, QQ27, and QQ28 Demonstrate That QQ58 and QQ27 Are More Potent Than QQ28. The IC_{50} values of QQ58, QQ27, and QQ28 were determined against human breast and prostate carcinoma tumor cell lines. As shown in Table 2, the cytotoxicity in both cell lines followed the same pattern, with the IC_{50} potency values increasing in the order QQ28 > QQ27 > QQ58. For QQ28 and QQ58, the cytotoxicity in DU-145 was higher than in MDA-MB-231. We have observed a similar high sensitivity to other quinolones in DU-145 cells in comparison with MDA-MB-231.[14]

The Antiproliferative and Chromosomal Effects of QQ58, QQ27, and QQ28 Show That QQ58 and QQ27 Are More Potent Than QQ28. Nonmammalian organisms are attractive supplements to conventional *in vivo* models, because the key cellular pathways are conserved throughout the animal kingdom. We have examined early stage sea urchin embryos as a novel *in vivo* model that allows rapid assessment of drug effects over many cell cycles in much less time than in other animal models or in cultured human tumor cells. To date we have evaluated the *in vivo* effects of anticancer agents from diverse groups, such as alkylators, DNA-interactive natural products, and telomere- and telom-

[14] E. Izbicka, manuscript in preparation.

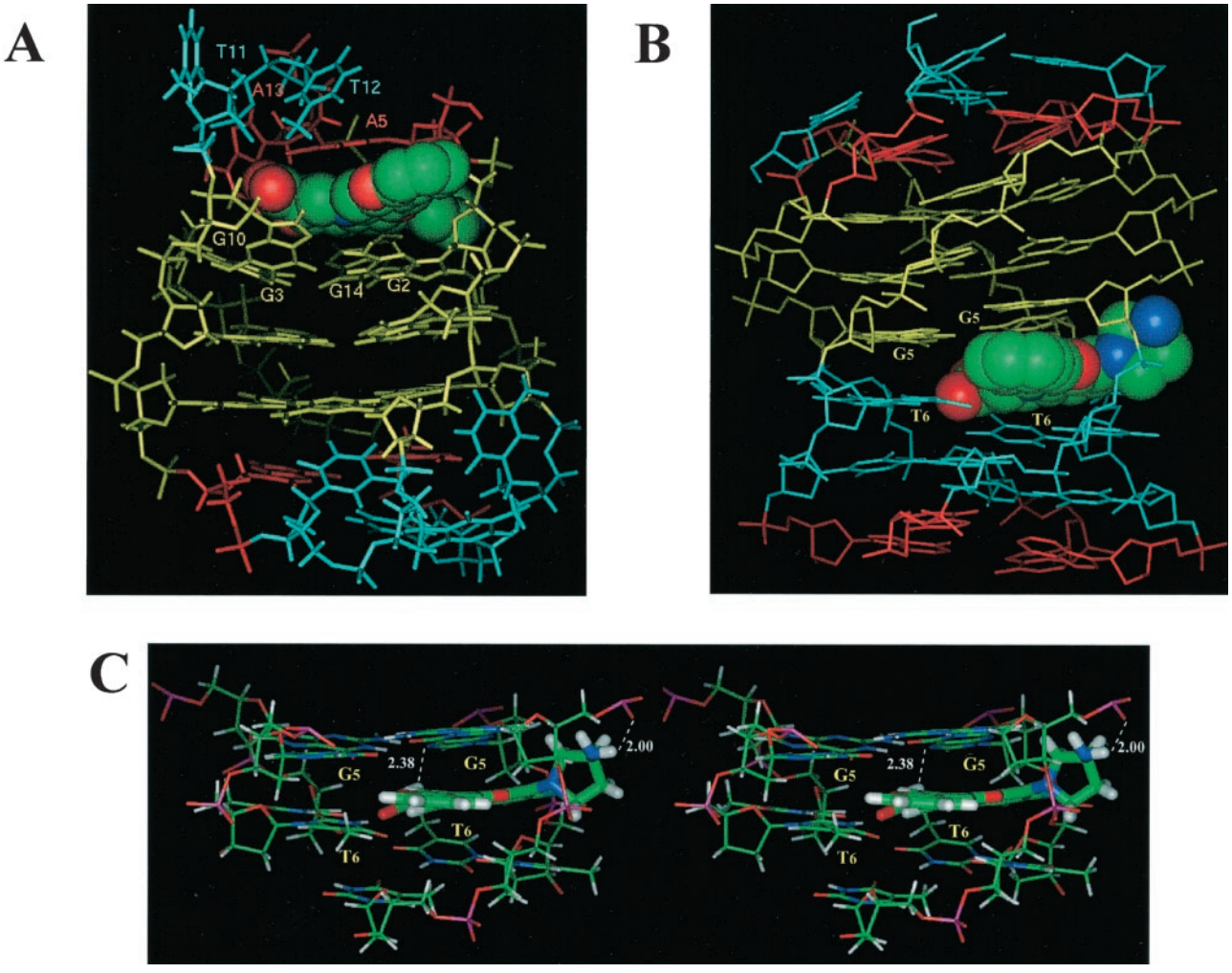

Fig. 8. Molecular modeling of the d[$AG_3(T_2AG_3)_3$]-QQ58 (*A*) and d[$TAG_3T_2A]_4$-QQ58 (*B* and *C*) complexes. *A,* structure of the d[$AG_3(T_2AG_3)_3$]-QQ58 complex in the final model after energy minimization. The G-quadruplex structure is shown as a stick model with compound QQ58 in color by atom type Corey-Pauling Koltun model. The proposed intercalation sites (*yellow*) are labeled. *B,* structure of the d[$TAG_3T_2A]_4$-QQ58 complex in the final model after energy minimization. Coloring is as in *A*. *C,* stereo representation of the proposed binding mode of QQ58 in complex with parallel-stranded G-quadruplex shown in color by atom type. The *white dotted lines* show the hydrogen bonding distances in Å. The G-quadruplex complex is clipped to afford a better view of the intercalation site.

erase-interactive agents, including a telomere mimic. We determined the effects of these agents on cellular proliferation using a new quantitative assay and on chromosome morphology. The specific and reproducible effects of many of these drugs correlated with the detection of similar effects in tumor cells (54, 55, 61–63).

In this study, we evaluated the *in vivo* effects of 1 μM of QQ28, QQ27, and QQ58 in developing sea urchin embryos. Preliminary dose-dependence tests have shown that these concentrations are subtoxic and compatible with the assays. Antiproliferative effects of the agents were assessed by examining the morphology of the embryos cultured for 10 and 24 h in the presence of the three quinolones. Photomicrographs (Fig. 10*A*) show that at 10 h all of the embryos are still within fertilization coats. The control group and QQ28-treated embryos appear normal with well-defined blastocoels. Cleavage is delayed in QQ27- and QQ58-treated embryos, so there are fewer cells, and a blastocoel has not yet formed. At 24 h (Fig. 10*B*) all of the embryos have hatched and are swimming, which suggests lack of major toxicity of the examined compounds. The control group and QQ28-treated embryos appear normal with well-defined blastocoels into which PMCs have ingressed at the vegetal pole (seen as the thicker layer of cells in the bottom of the embryos). Invagination of the vegetal pole has begun in the control group and the QQ28-treated embryos. Because of the cleavage delay in the QQ27- and QQ58-treated embryos, the embryos are smaller and there are fewer cells. Additionally, the blastocoels appear to be abnormally filled with cells, and there does not appear to be a concentration of PMCs at a well-defined vegetal pole. The antiproliferative effect of QQ58 is apparently greater than that of QQ27, and this difference is more noticeable at 10 h than at the later time point at 24 h.

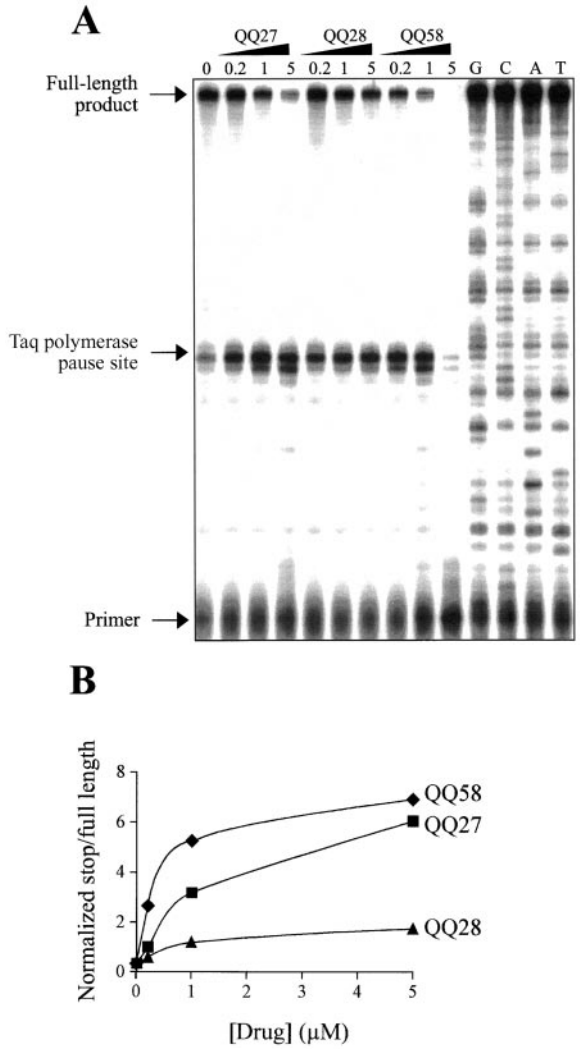

Fig. 9. Differential effects of QQ27, QQ28, and QQ58 on DNA synthesis arrest by G-quadruplex structure. *A,* autoradiogram of the sequencing gel showing Taq polymerase primer extension arrest at the G-quadruplex site in the presence of QQ58, QQ27, and QQ28. *Lanes G, C, A,* and *T* are DNA sequencing lanes. *B,* quantitation of the sequencing gel shown in *A*. The drug concentrations are plotted against the normalized ratios of the band intensity of the G-quadruplex pause site and the band intensity of the full-length product.

Chromosome-specific effects of the agents were determined using high-power fluorescence microscopy. Although a single focal plane is exceeded at magnifications greater than ×400, resolution of mitotic chromosomes in all phases of mitosis is possible. Both the nuclei and chromosomes may be visualized in bright red over a dark background with fluorescence optics (green excitation), with very little photobleaching. We have used this method to assess chromosome-specific effects of QQ28, QQ27, and QQ58 in 10-h embryos cultured in the continuous presence of the compounds. The 10-h embryos have been chosen as more representative than the 24-h ones because at 10 h the embryos are actively dividing and there is the most chromosomal activity. Fig. 11 (top left panel) shows representative mitotic chromosomes in a control (nontreated) embryo at 10 h after fertilization. The condensed mitotic chromosomes stain more deeply than the less condensed interphase nuclei in the background. Many metaphase chromosomes are observed in typical linear arrangements on metaphase plates. During anaphase the chromosomes separate and move to opposite poles cleanly with very little "tailing" of chromosome arms on the mitotic spindle. Telophase chromosomes are observed as two small, dense concentrations of mitotic chromosomes at opposite poles, where they will decondense into interphase nuclei. As additionally shown in Fig. 11, not only the control but also QQ28-treated embryos show the normal "tight" mitotic chromosomes among a larger number of nuclei. On the other hand, the QQ27- and QQ58-treated embryos show a reduced number of nuclei, consistent with a growth delay. The nuclei are larger and more diffuse. The mitotic chromosomes are more diffuse and segregate abnormally, often to multiple poles, and end-to-end fusions are often observed. These results are consistent with the cleavage delay, and fewer cells are seen in the live embryos.

Table 2 Cytotoxicity of novel quinolones against human tumor cell lines

Compound	IC_{50} (μM)	
	MDA-MB-231	DU-145
QQ58	0.15	0.07
QQ27	1.25	1.86
QQ28	>20	5.77

Discussion

In this study we have identified a new structural motif for a ligand with G-quadruplex interaction that results in biological effects associated with G-quadruplex-interactive compounds. The initial lead compound was a quinobenzoxazine, which derived its structural origin from the well-known fluoroquinolone antibiotics (see Fig. 12), typified by norfloxacin. Researchers at Abbott Laboratories, Abbott Park, IL demonstrated that this quinobenzoxazine compound could be converted into a mammalian cytotoxic agent by expansion of the dicyclic quinolone to the tetracyclic quinobenzoxazine (A-62176), which was shown to be a topoisomerase II poison (64). The same structural elements (planarity, amphoteric nature) can then be used as a basis to design an even more expanded ring system (quinophenoxazine) that is now a G-quadruplex-interactive drug (QQ58) that causes biological effects associated with G-quadruplex-interactive compounds.

Comparison of Complexes of A-62176 and QQ58 with the Topoisomerase II-DNA Complex and the G-Quadruplex Structure. Whereas both norfloxacin and A-62176 target gyrase and topoisomerase II-DNA complexes to produce poisoned complexes in which these drugs stabilize the covalently linked protein-DNA complexes, QQ58 has lost this property (see Fig. 3) but is instead able to recognize and bind quite specifically to G-quadruplex structures. The quinoben-

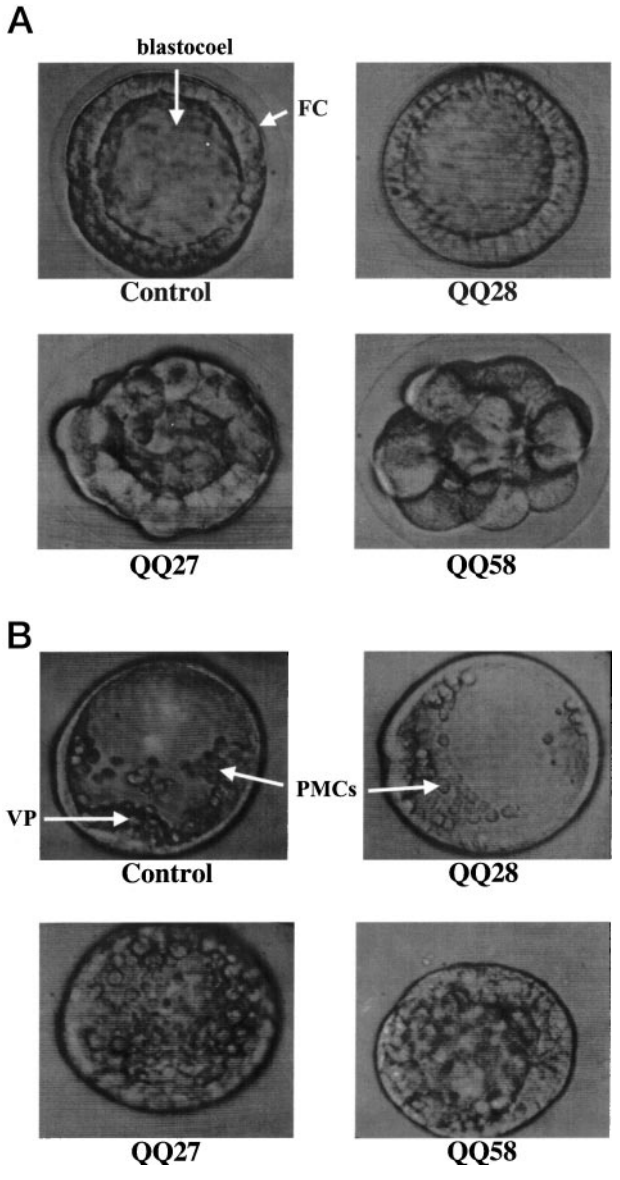

Fig. 10. Effects of FQPs on proliferation dynamics of early sea urchin embryos. The embryos were cultured in the presence of FQPs or DMSO (*control*) for 10 h (*A*) or 24 h (*B*), pelleted by centrifugation, and video micrographed as described in "Materials and Methods." *A,* 10 h: the thin surrounding coat elevated away from the surface of the embryo is the fertilization coat (*FC*), which is present in all embryos. The thick layer below the FC is the cellular layer of the early blastula embryo. At 10 h, there are 400–500 cells in it. These layers are fully formed in control and QQ28-treated embryos. There are fewer and larger cells in the QQ27- and QQ58-treated embryos, so the layer is thicker and not fully formed. The cellular layer surrounds the blastocoel, the fluid-filled cavity of the early embryo into which cells of the cellular layer will move during the formation of the larval gut. *B,* 24 h: no FCs are present in any of the embryos. This demonstrates that toxicity is not found at 1 μM because to hatch out of the FCs the embryos must synthesize a specific protease, hatching enzyme that degrades the FCs. Hatching occurs at ~15 h in these embryos. In addition, all embryos produce cilia and begin to swim at the normal time, shortly before hatching, thus demonstrating their viability, although there are fewer cells in the QQ27- and QQ28-treated cells. In control and QQ28-treated embryos, development is normal. There is a thin cellular layer composed of ~1000 cells that surrounds the blastocoel. Cells from the cellular layer have moved into the blastocoels. They are the PMCs. At 7:00 in the control embryo and at 9:00 in the QQ28-treated embryo the cellular layer has begun to invaginate to form the larval gut. At this stage it can be labeled the VP. In the QQ27- and QQ58-treated embryos, cell division has proceeded since 10 h, and there are obviously more cells. However, the embryos lack definitive blastocoels because cells seem to abnormally fill the blastocoels. Well-organized PMCs and obvious VPs are not present, although the thickened, flattened cellular layer in the QQ58-treated embryo at 3:00 could be a VP.

zoxazine molecule A-62176 requires divalent cations such as Mg^{2+} to form a stable complex with DNA, and we have proposed a 2:2 drug:Mg^{2+} model for the complex with both duplex DNA and the topoisomerase II-DNA complex (65). In contrast to this requirement for divalent cation, the FQP does not require metals for its interaction with either the intra- or intermolecular G-quadruplex structure, and we have more direct and precise structural information on the structure of the complex in which only one molecule of the FQP binds to a single G-quadruplex molecule, in contrast to the two in the model of the A-62176-DNA–topoisomerase II complex (65).

It seems likely that QQ58, like A-62176, will bind nonspecifically by an intercalative mechanism to duplex DNA, *i.e.,* similar to that in which divalent cations are not involved. An important objective is to design G-quadruplex-interactive compounds belonging to the FQP group that clearly differentiate between duplex and G-quadruplex DNA.

Molecular Recognition of the G-Quadruplex Structure by QQ58. Despite the contrasts in the molecular targets (duplex topoisomerase II *versus* G-quadruplex structures) of A-62176 and QQ58, there are common molecular features of both molecules that appear critical for recognition of unique features of the two different receptors. These are the amphoteric nature of both molecules, the intramolecular separation distance of the positive and negative charges, and the planar nature of both the quinobenzoxazine and FQP molecules. For the FQP molecule QQ58, the carboxylic acid and amino group of the pyrrolidine are both involved in donor-acceptor interactions with N7 of guanine in the external tetrad and the anionic backbone of the G-quadruplex structure, respectively. The charge separation of the amphoteric groups on QQ58 is precisely that required for in-register interaction with the complementary groups on the G-quadruplex structure. This observation provides the insight into why even norfloxacin shows some modest telomerase inhibition. However, because norfloxacin and A-62176 have minimal stacking interactions within the G-tetrad-thymine step of the G-quadruplex structures, there is presumably insufficient π-π interaction to adequately stabilize the complex. The relative importance of the charge-charge interactions and the stacking is illustrated by the comparative modeling and biological studies of QQ58, QQ27, and QQ28. Whereas steric disruption of the two in-register donor-acceptor pairs in the QQ28-G-quadruplex interactions almost completely eliminates G-quadruplex binding and biological activity, the sterically tolerated ethylester of QQ27 still permits one of two H-bonds and may partially make up for the post-electrostatic interactions by increasing the van der Waals interactions, thus permitting residual G-quadruplex binding and biological activity that is almost as good as QQ58. Most important, our QQ58-G-quadruplex model, which is based on ^{1}H NMR and photocleavage data, along with molecular modeling, accounts fully for the modulation of

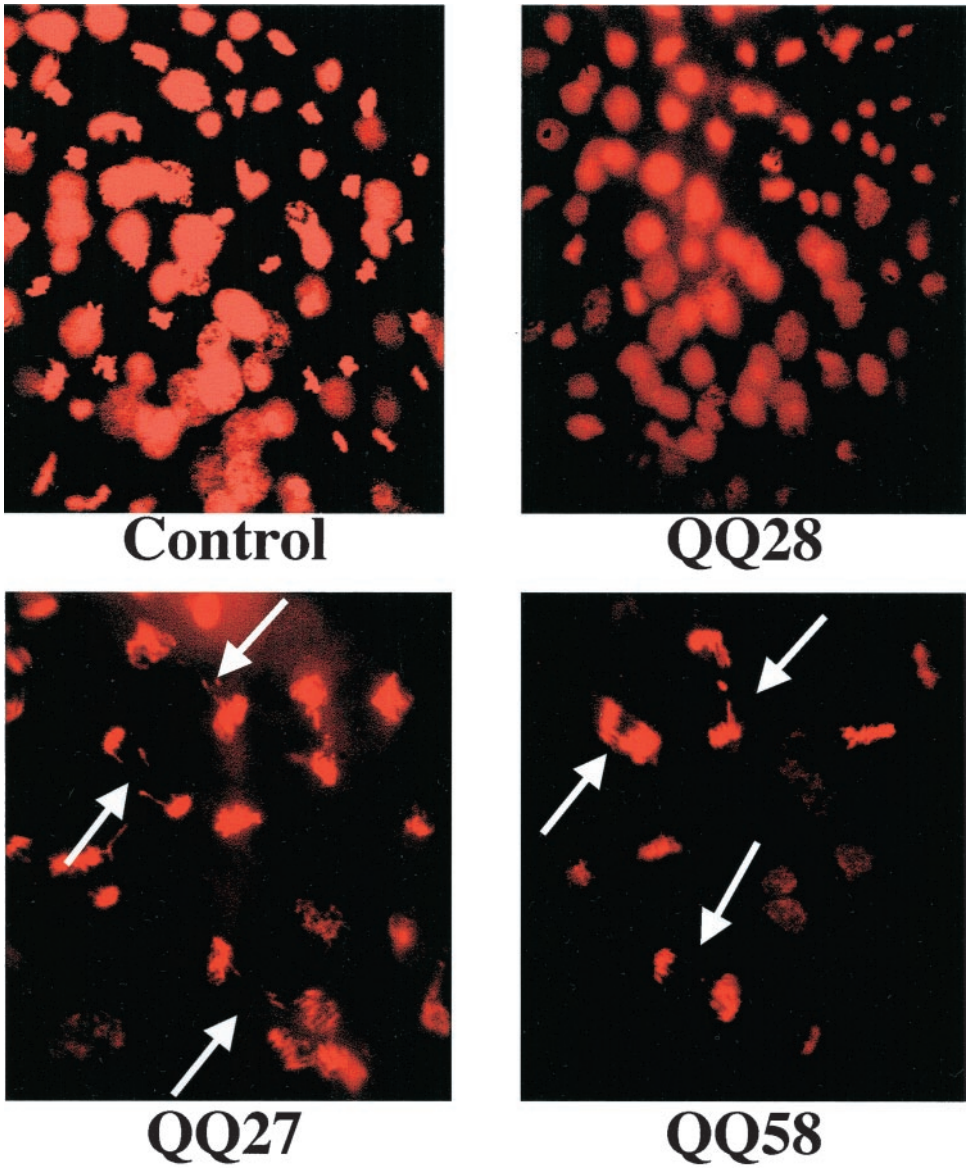

Fig. 11. Chromosomal effects of FQPs in early sea urchin embryos. The embryos were cultured in the presence of FQPs or DMSO (*control*) for 10 h and pelleted by centrifugation. The nuclei were stained by Feulgen reaction and the chromatin was visualized as described under "Materials and Methods." Chromosomal bridges are marked with *arrows*.

activity of QQ27 and QQ28 and also provides an important starting point for the design of more potent compounds.

Biological Effects of the FQPs. The three quinolones QQ28, QQ27, and QQ58 examined in this study exhibit different modes of interaction with G-quadruplexes and effects on topoisomerase II activity. Interestingly, QQ28, which neither interacts with G-quadruplex nor poisons topoisomerase II, showed the lowest cytotoxicity in two model human tumor cell lines *in vitro* and had no major antiproliferative effect on developing sea urchin embryos *in vivo*. The G-quadruplex-interactive compounds QQ58 and QQ27, which do not poison topoisomerase II, showed increased cytotoxicity in human tumor cells and sea urchin embryos. In both systems, the antiproliferative effects of QQ58 were more potent than those of QQ27.

Although QQ27 and QQ58 significantly delayed growth of the embryos at the early stages, the development of the embryos was not largely impaired, which is consistent with a lack of major cytotoxic effects. Under subtoxic conditions, we were able to observe chromosome end fusions induced only by these compounds. The chromosomal abnormality exhibited specifically by embryos treated with QQ27 and QQ58 is an apparent end-to-end adherence of anaphase and telophase chromosomes. The end-to-end adhesions are manifested in the form of anaphase chromosomes that often extend from pole to pole of the mitotic spindle. These effects are very similar to the chromosomal fusions that result from a mutation in the telomerase template in *Tetrahymena* (66) and a dominant negative mutation in the telomere binding protein TRF2 in HTC75 cells (67).

The end-to-end adherence of chromosomes is observed in embryos treated with structurally dissimilar telomere- and telomerase-interactive agents designed to target very different sites in the telomere-telomerase complex. We have

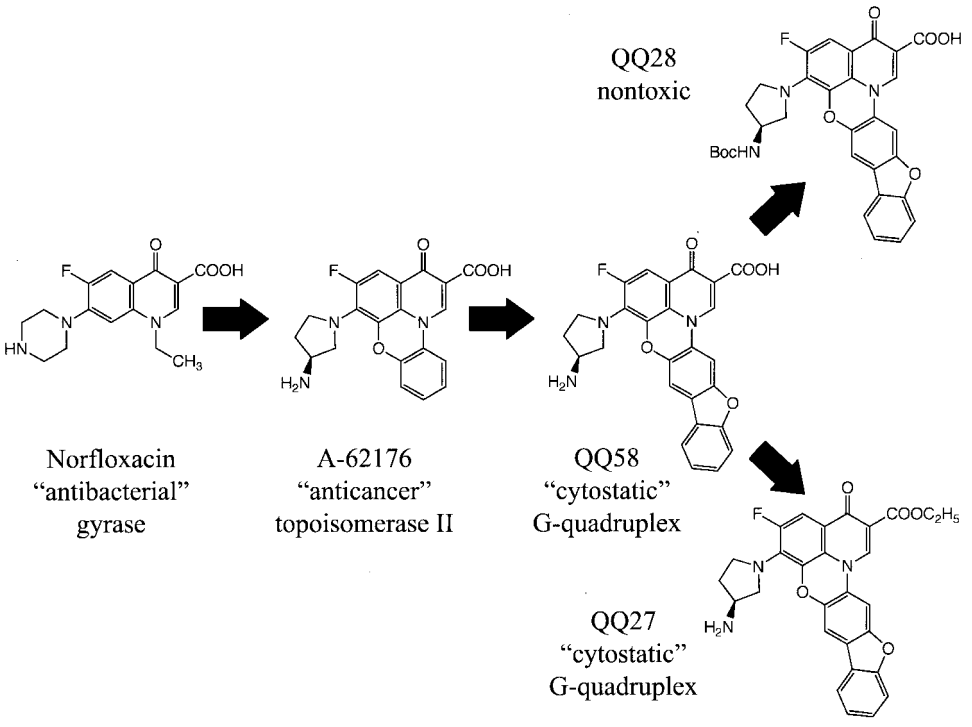

Fig. 12. Evolution of QQ58 from norfloxacin and effects of QQ58 structural modification.

found that the G-quadruplex-interactive porphyrin TMPyP4 showed the most potent chromosome destabilizing properties with no significant inhibition of DNA synthesis (54). Because the isomeric porphyrin TMPyP2, which does not show stacking interactions with G-quadruplex, has not demonstrated similar effects in sea urchins and other systems examined to date, the telomere effects of TMPyP4 might be related to stabilization and/or *de novo* formation of G-quadruplex in cells. This specific chromosomal effect has also been induced by an oligonucleotide telomere mimic but not the scrambled sequence (54), and by other agents, of which the mechanisms of action might involve regulation of telomere maintenance (62, 63).

By analogy, the chromosome destabilizing activity of QQ27 and QQ58 suggests that these compounds might also affect telomere integrity. The results suggest that the G-quadruplex interactions are linked with the ability of FQP to induce chromosome destabilization. Poisoning of topoisomerase II does not apparently play a role in the process, because QQ58 and QQ27, which do not poison topoisomerase II, stimulated end-to-end adherence of chromosomes. We have demonstrated[15] that the quinolones can stabilize, but do not stimulate, *de novo* formation of G-quadruplex. Thus, the present results imply that G-quadruplex-like structures may well exist *in vivo*. Additional investigation of this issue is warranted.

Acknowledgments

We thank the other members of the National Cooperative Drug Design Group team in Austin and San Antonio for valuable discussions. We also thank Dr. David Bishop, College of Pharmacy, The University of Arizona, Tucson, AZ for preparing, proofreading, and editing the final version of the manuscript, figures, schemes, and tables.

[15] A. Rangan, unpublished observations.

References

1. Wang, J. C. DNA topoisomerases. Annu. Rev. Biochem., *65:* 635–692, 1996.

2. Reece, R. J., and Maxwell, A. DNA gyrase: structure and function. CRC Crit. Rev. Biochem. Mol. Biol., *26:* 335–375, 1991.

3. Nitiss, J. L. Investigating the biological functions of DNA topoisomerases in eukaryotic cells. Biochim. Biophys. Acta, *1400:* 63–81, 1998.

4. Yamakuchi, M., Nakata, M., Kawahara, K., Kitajima, I., and Maruyama, I. New quinolones, ofloxacin and levofloxacin, inhibit telomerase activity in transitional cell carcinoma cell lines. Cancer Lett., *119:* 213–219, 1997.

5. Zeng, Q., Kwok, Y., Kerwin, S. M., Mangold, G., and Hurley, L. H. Design of new topoisomerase II inhibitors based upon a quinobenzoxazine self-assembly model. J. Med. Chem., *41:* 4273–4278, 1998.

6. Sun, D., Thompson, B., Cathers, B. E., Salazar, M., Kerwin, S. M., Trent, J. O., Jenkins, T. C., Neidle, S., and Hurley, L. H. Inhibition of human telomerase by a G-quadruplex-interactive compound. J. Med. Chem., *40:* 2113–2116, 1997.

7. Perry, P. J., Read, M. A., Davies, R. T., Gowan, S. M., Reszka, A. P., Wood, A. A., Kelland, L. R., and Neidle, S. 2,7-Disubstituted amidofluorenone derivatives as inhibitors of human telomerase. J. Med. Chem., *42:* 2679–2684, 1999.

8. Harrison, R. J., Gowan, S. M., Kelland, L. R., and Neidle, S. Human telomerase inhibition by substituted acridine derivatives. Bioorg. Med. Chem. Lett., *9:* 2463–2468, 1999.

9. Read, M. A., Wood, A. A., Harrison, R. J., Gowan, S. M., Kelland, L. R., Dosanjh, H. S., and Neidle, S. Molecular modeling studies on G-quadruplex complexes of telomerase inhibitors: structure-activity relationships. J. Med. Chem., *42:* 4538–4546, 1999.

10. Read, M., Harrison, R. J., Romagnoli, B., Tanious, F. A., Gowan, S. H., Reszka, A. P., Wilson, W. D., Kelland, L. R., and Neidle, S. Structure-based design of selective and potent G-quadruplex-mediated telomerase inhibitors. Proc. Natl. Acad. Sci. USA, *98:* 4844–4849, 2001.

11. Wheelhouse, R. T., Sun, D., Han, H., Han, F. X., and Hurley, L. H. Cationic porphyrins as telomerase inhibitors: the interaction of tetra(*N*-methyl-4-pyridyl)porphine with quadruplex DNA. J. Am. Chem. Soc. *120:* 3261–3262, 1998.

12. Han, F. X., Wheelhouse, R. T., and Hurley, L. H. Interactions of TMPyP4 and TMPyP2 with quadruplex DNA. Structural basis for the differential effects on telomerase inhibition. J. Am. Chem. Soc., *121:* 3561–3570, 1999.

13. Han, H., Rangan, A., Langley, D. R., and Hurley, L. H. Selective interaction of cationic porphyrins with G-quadruplex structures. J. Am. Chem. Soc. *123:* 8902–8913, 2001.

14. Riou, J-F., Mailliet, P., Laoui, A., Renou, E., Petigenet, O., Guittat, L., and Mergny, J-L. Apoptosis, cell senescence, and telomere shortening induced by a new series of specific G-quadruplex DNA ligand. Proc. Am. Assoc. Cancer Res. *42:* 837, 2001.

15. Koeppel, F., Riou, J-F., Laoui, A., Malliet, P., Arimondo, P. B., Labit, D., Petigenet, O., Hélène, C., and Mergny, J-L. Ethidium derivatives bind to G-quartets, inhibit telomerase, and act as fluorescent probes for quadruplexes. Nucleic Acids Res., *29:* 1087–1096, 2001.

16. Gowan, S. M., Brunton, L., Valenti, M., Heald, R., Read, M. A., Harrison, J. R., Stevens, M. F. G., Neidle, S., and Kelland, L. R. Preclinical antitumor properties of G-quadruplex-interactive small molecule inhibitors of telomerase. Proc. Am. Assoc. Cancer Res., *42:* 86, 2001.

17. Gellert, M., Lipsett, M. N., and Davies, D. R. Helix formation by guanylic acid. Proc. Natl. Acad. Sci. USA, *48:* 2013–2018, 1962.

18. Henderson, E., Hardin, C. C., Walk, S. K., Tinoco, K., Jr., and Blackburn, E. H. Telomeric DNA oligonucleotides form novel intramolecular structures containing guanine-guanine base pairs. Cell, *51:* 899–908, 1987.

19. Sundquist, W. I., and Klug, A. Telomeric DNA dimerizes by formation of guanine tetrads between hairpin loops. Nature (Lond.), *342:* 825–829, 1989.

20. Sundquist, W. I., and Heaphy, S. Evidence for interstrand quadruplex formation in the dimerization of human immunodeficiency virus 1 genomic RNA. Proc. Natl. Acad. Sci. USA, *90:* 3393–3397, 1993.

21. Sen, D., and Gilbert, W. Formation of parallel four-stranded complexes by guanine-rich motifs in DNA and its implications for meiosis. Nature (Lond.), *334:* 364–366, 1988.

22. Hammond-Kosack, M. C., Kilpatrick, M. W., and Docherty, K. Analysis of DNA structure in the human insulin gene-linked polymorphic region *in vivo*. J. Mol. Endocrinol., *9:* 221–225, 1992.

23. Murchie, A. I., and Lilley, D. M. Retinoblastoma susceptibility genes contain 5′ sequences with a high propensity to form guanine-tetrad structures. Nucleic Acids Res., *20:* 49–53, 1992.

24. Hurley, L. H. DNA and associated targets for drug design. J. Med. Chem., *32:* 2027–2033, 1989.

25. Giraldo, R., and Rhodes, D. The yeast telomere-binding protein RAP1 binds to and promotes the formation of DNA quadruplexes in telomeric DNA. EMBO J., *13:* 2411–2420, 1994.

26. Fang, G., and Cech, T. R. The β-subunit of *Oxytricha* telomere-binding protein promotes G-quartet formation by telomeric DNA. Cell, *74:* 875–885, 1993.

27. Arimondo, P. B., Riou, J. F., Mergny, J. L., Tazi, J., Sun, J. S., Garestier, T., and Hélène, C. Interaction of human DNA topoisomerase I with G-quartet structures. Nucleic Acids Res., *28:* 4832–4838, 2000.

28. Hanakahi, L. A., Sun, H., and Maizels, N. High affinity interactions of nucleolin with G-G-paired rDNA. J. Biol. Chem., *274:* 15908–15912, 1999.

29. Oliver, A. W., Bogdarina, I., and Kneale, G. G. Preferential binding of Fd gene 5 protein to tetraplex nucleic acid structures. J. Mol. Biol., *301:* 575–584, 2000.

30. Harrington, C., Lan, Y., and Akman, S. A. The identification and characterization of G4-DNA resolvase activity. J. Biol. Chem., *272:* 24631–24636, 1997.

31. Gilson, E., Roberge, M., Giraldo, R., Rhodes, D., and Glasser, S. M. Distortion of the DNA double helix by RAP1 at silencers and multiple telomeric binding-sites. J. Mol. Biol., *231:* 293–310, 1993.

32. Suzuki, N., Shimamoto, A., Imamura, O., Kuromitsu, J., Kitao, S., Goto, M., and Furuichi, Y. DNA helicase activity in Werner's syndrome gene product synthesized in a baculovirus system. Nucleic Acids Res., *25:* 2973–2978, 1997.

33. Sun, H., Karow, J. K., Hickson, I. D., and Maizels, N. The Bloom's syndrome helicase unwinds G4 DNA. J. Biol. Chem., *273:* 27587–27592, 1998.

34. Sun, H., Bennett, R. J., and Maizels, N. The *Saccharomyces cerevisiae* Sgs1 helicase efficiently unwinds G-G paired DNAs. Nucleic Acids Res., *27:* 1978–1984, 1999.

35. Schaffitzel, C., Berger, I., Postberg, J., Hanes, J., Lipps, H. J., and Plückthu, A. *In vitro* generated antibodies specific for telomeric guanine-quadruplex DNA react with *Stylonychia lemnae* macronuclei. Proc. Natl. Acad. Sci. USA, *98:* 8572–8577, 2001.

36. Izbicka, E., Wheelhouse, R. T., Raymond, E., Davidson, K. K., Lawrence, R. A., Sun, D., Windle, B. E., Hurley, L. H., and Von Hoff, D. D. Effects of cationic porphyrins as G-quadruplex-interactive agents in human tumor cells. Cancer Res., *59:* 639–644, 1999.

37. Mergny, J-L., and Hélène, C. G-quadruplex DNA: a target for drug design. Nat. Med., *4:* 1366–1367, 1998.

38. Han, H., and Hurley, L. H. G-quadruplex DNA: a potential target in anticancer drug design. Trends Pharmacol. Sci., *21:* 136–142, 2000.

39. Hurley, L. H., Wheelhouse, R. T., Sun, D., Kerwin, S. M., Salazar, M., Fedoroff, O. Yu., Han, F. X., Han, H., Izbicka, E., and Von Hoff, D. D. G-quadruplexes as targets for drug design. Pharmacol. Ther., *85:* 141–158, 2000.

40. Kerwin, S. M. G-quadruplex DNA as a target for drug design. Curr. Pharm. Des., *6:* 441–471, 2000.

41. Jenkins, T. C. Targeting multi-stranded DNA structures. Curr. Med. Chem., *7:* 99–115, 2000.

42. Sun, D., and Hurley, L. H. Targeting telomeres and telomerase. *In:* J. B. Chaires, and M. J. Waring (eds.), Methods in Enzymology, Vol. 340, pp. 573–592. San Diego: Academic Press, 2001.

43. Raymond, E., Sun, D., Chen, S-F., Windle, B., and Von Hoff, D. D. Agents that target telomerase and telomeres. Curr. Opin. Biotechnol., *7:* 583–591, 1996.

44. Kelland, L. R. Telomerase: biology and phase 1 trials. Lancet, *2:* 95–102, 2001.

45. Bearss, D. J., Hurley, L. H., and Von Hoff, D. D. Telomere maintenance mechanisms as a target for drug development. Oncogene, *19:* 6632–6641, 2000.

46. Kwok, Y., Zeng, Q., and Hurley, L. H. Structural insight into a quinolone-topoisomerase-DNA complex: evidence for a 2:2 quinobenzoxazine:Mg^{2+} self-assembly complex in the presence of topoisomerase II. Biol. Chem., *274:* 17226–17235, 1999.

47. Sun, D., Hurley, L. H., and Von Hoff, D. D. Telomerase assay using biotinylated-primer extension and magnetic separation of the products. BioTechniques, *25:* 1046–1051, 1998.

48. Han, H., Hurley, L. H., and Salazar, M. A DNA polymerase stop assay for G-quadruplex-interactive compounds. Nucleic Acids Res., *27:* 537–542, 1999.

49. Fedoroff, O. Yu., Salazar, M., Han, H., Chemeris, V. V., Kerwin, S. M., and Hurley, L. H. NMR-based model of a telomerase-inhibiting compound bound to G-quadruplex DNA. Biochemistry, *37:* 12367–12374, 1998.

50. Wang, Y., and Patel, D. J. Solution structure of the human telomeric repeat $d[AG_3(T_2AG_3)_3]$ G-tetraplex. Structure (Lond.), *1:* 263–282, 1993.

51. INSIGHT II Molecular Modeling, Molecular Simulations Inc., San Diego, 2000.

52. Luty, B. A., Wasserman, Z. R., Stouten, P. F. W., Hodge, C. N., Zacharias, M., and McCammon, J. A. A molecular mechanics/grid method for the evaluation of ligand-receptor interactions. J. Comput. Chem., *16:* 454–464, 1995.

53. Mossman, T. Rapid colorimetric assay for cellular growth and survival: application to proliferation and cytotoxicity assays. J. Immunol. Methods, *65:* 55–63, 1983.

54. Izbicka, E., Nishioka, D., Marcell, V., Raymond, E., Davidson, K. K., Lawrence, R. A., Wheelhouse, R. T., Hurley, L. H., Wu, R. S., and Von Hoff, D. D. Telomere-interactive agents affect proliferation rates and induce

chromosomal destabilization in sea urchin embryos. Anti-Cancer Drug Des., *14:* 355–365, 1999.

55. Nishioka, D., Marcell, V., Cunningham, M., Khan, M., Von Hoff, D., and Izbicka, E. The use of early sea urchin embryos in anticancer drug testing. Methods in Molecular Medicine, Humana Press, in press, 2001.

56. Chu, D. T. W., and Maleczka, R. E., Jr. Synthesis of 4-oxo-4H-quino-[2: 3,4-i, j][1,4]benoxazine-5-carboxylic acid derivatives. J. Heterocycl. Chem., *24:* 453–456, 1987.

57. Sahai, B. M., and Kaplan, J. G. A quantitative decatenation assay for type II topoisomerases. Anal. Biochem., *156:* 364–379, 1986.

58. Marini, J. C., Miller, K. G., and Englund, P. T. Decatenation of kinetoplast DNA by topoisomerases. J. Biol. Chem., *225:* 4976–4979, 1980.

59. Zahler, A. M., Williamson, J. R., Cech, R. R., and Prescott, D. M. Inhibition of telomerase by G-quartet DNA structures. Nature (Lond.), *350:* 718–720, 1991.

60. Weitzmann, M. N., Woodford, K. J., and Usdin, K. The development and use of a DNA polymerase arrest assay for the evaluation of parameters affecting intrastrand tetraplex formation J. Biol. Chem., *271:* 20958–20964, 1996.

61. Izbicka, E., Nishioka, D., Wu, R., Von Hoff, D., Weitman, S., and Hurley, L. H. Antiproliferative and chromosome destabilizing effects of novel quinolones. Proc. Am. Assoc. Cancer Res., *40:* 16, 1999.

62. Nishioka, D., Wu, R., Rha, S., Von Hoff, D., and Izbicka, E. HMAF (6-hydroxymethylacylfulvene, MGI 114) induces chromosome destabilization in developing sea urchin embryos. Proc. Am. Assoc. Cancer Res., *40:* 3, 1999.

63. Nishioka, D., Wu, R., Von Hoff, D., and Izbicka, E. Chromosome effects of ecteinascidin ET-743 (ET-743) in a sea urchin embryo model. Proc. Am. Assoc. Cancer Res., *40:* 300, 1999.

64. Permana, P. A., Snapka, R. M., Shen, L. L., Chu, D. T. W., Clement, J. J., and Plattner, J. J. Quinobenzoxazines: a class of novel antitumor quinolones and potent mammalian DNA topoisomerase II catalytic inhibitors. Biochemistry, *33:* 11333–11339, 1994.

65. Fan, J-Y., Sun, D., Yu, H., Kerwin, S. M., and Hurley, L. H. Self-assembly of a quinobenzoxazine-Mg^{2+} complex on DNA: a new paradigm for the structure of a drug-DNA complex and implications for the structure of the quinolone bacterial gyrase-DNA complex. J. Med. Chem., *38:* 408–424, 1995.

66. Kirk, K., Harmon, B., Reichardt, I., Sedat, J., and Blackburn, E. Block in anaphase chromosome separation caused by telomerase template mutation. Science (Wash. DC), *275:* 1478–1481, 1997.

67. van Steensel, B., Smogorzewska, A., and de Lange, T. TRF2 protects human telomeres from end-to-end fusions. Cell, *92:* 401–413, 1998.